Copy 271
RM A51H20

NACA

RESEARCH MEMORANDUM

AN INVESTIGATION OF THE DRAG AND PRESSURE RECOVERY OF A SUBMERGED INLET AND A NOSE INLET IN THE TRANSONIC FLIGHT RANGE WITH FREE-FALL MODELS

By James Selna and Bernard A. Schlaff

Ames Aeronautical Laboratory
Moffett Field, Calif.

NATIONAL ADVISORY COMMITTEE
FOR AERONAUTICS

WASHINGTON

December 28, 1951

NATIONAL ADVISORY COMMITTEE FOR AERONAUTICS

RESEARCH MEMORANDUM

AN INVESTIGATION OF THE DRAG AND PRESSURE RECOVERY OF A SUBMERGED INLET AND A NOSE INLET IN THE TRANSONIC FLIGHT RANGE WITH FREE-FALL MODELS

By James Selna and Bernard A. Schlaff

SUMMARY

The drag and pressure recovery of an NACA submerged-inlet model and an NACA series I nose-inlet model were investigated in the transonic flight range. The tests were conducted over a mass-flow-ratio range of 0.4 to 0.8 and a Mach number range of about 0.8 to 1.10 employing large-scale recoverable free-fall models.

The results indicate that the Mach number of drag divergence of the inlet models was about the same as that of a basic model without inlets. The external drag coefficients of the nose-inlet model were less than those of the submerged-inlet model throughout the test range. The difference in drag coefficient based on the maximum cross-sectional area of the models was about 0.02 at supersonic speeds and about 0.015 at subsonic speeds. For a hypothetical airplane with a ratio of maximum fuselage cross-sectional area to wing area of 0.06, the difference in airplane drag coefficient would be relatively small, about 0.0012 at supersonic speeds and about 0.0009 at subsonic speeds. Additional drag comparisons between the two inlet models are made considering inlet incremental and additive drag.

The maximum pressure recovery of the submerged inlet at subsonic speeds agrees well with previous results. The maximum pressure recovery diminished when supersonic speeds prevailed on the inlet ramp. The amount of decrease was slight, being of the order of that anticipated for the total-pressure loss through a normal shock at the maximum ramp Mach numbers. The variation of the pressure recovery with mass-flow ratio is in reasonable agreement with previous results.

INTRODUCTION

In order to evaluate the performance of an air inlet, it is necessary to know the drag associated with the use of the inlet as well as the pressure-recovery characteristics. Pressure-recovery data for inlets are generally available; however, only limited information is available on the drag of inlets.

Considerable pressure-recovery information on submerged inlets at subsonic speeds is given in references 1 to 5 and some data on the pressure recovery of submerged inlets in the transonic range are presented in references 6 to 8. Drag data on submerged inlets, however, are limited to a few tests at low subsonic speeds (references 1 and 2).

The pressure recovery of open nose inlets throughout the subsonic, transonic, and supersonic Mach number ranges is generally known (references 9 to 16). Drag information on open nose inlets at subsonic speeds are given in references 10, 11, and 12. Some drag data at supersonic speeds are given in references 13 and 14, and the only available data at transonic speeds are presented in references 13 and 16.

The purpose of the present investigation was to obtain comparative drag and pressure-recovery data for a submerged-inlet model and a nose-inlet model in the transonic speed range. The investigation was conducted with mass-flow ratios ranging from about 0.4 to 0.8 over a Mach number range of about 0.8 to 1.10. Preliminary results of this investigation, based on limited tests, were reported in reference 16, and are also included herein.

The investigation was conducted with large-scale, free-fall recoverable models in the desert regions of Edwards Air Force Base at Muroc, California.

SYMBOLS

A	total cross-sectional area of duct or ducts, square feet
A_x	component of area, normal to free stream, square feet
C_{D_T}	total drag coefficient $\left(\frac{D_T}{q_o S}\right)$, dimensionless
C_{D_I}	internal drag coefficient $\left(\frac{D_I}{q_o S}\right)$, dimensionless

C_{D_E} external drag coefficient $\left(C_{D_T} - C_{D_I}\right)$, dimensionless

C_{D_a} inlet incremental drag coefficient $\left(\frac{D_a}{q_o S}\right)$, dimensionless

C_{D_A} additive drag coefficient $\left(\frac{D_A}{q_o S}\right)$, dimensionless

d duct depth at duct entrance, inches

D_T total drag, pounds

D_E external drag $\left(D_T - D_I\right)$, pounds

D_I internal drag, pounds

D_A additive drag, pounds

D_a inlet incremental drag, pounds

D_f viscous drag, pounds

h boundary-layer parameter $\left[\frac{1}{H_o - p_o}\int_o^\delta (H_o - H)\, dy\right]$, inches

H total pressure, pounds per square foot

$\frac{H - p_o}{H_o - p_o}$ ram-recovery ratio, dimensionless

M Mach number, dimensionless

m mass flow, slugs per second

$\frac{m_1}{m_o}$ mass-flow ratio $\left(\frac{\rho_1 A_1 V_1}{\rho_o A_1 V_o}\right)$, dimensionless

p static pressure, pounds per square foot

q dynamic pressure $\left(\frac{1}{2}\rho V^2\right)$, pounds per square foot

q_c	impact pressure (H − p), pounds per square foot
S	cross-sectional area of model at maximum diameter, square feet
u	local velocity in boundary layer, feet per second
U	local velocity outside of boundary layer, feet per second
V	velocity, feet per second
y	distance away from model outer surface, inches
δ	boundary-layer thickness, inches
ρ	mass density of air, slugs per cubic foot

Subscripts

i	measured value at airspeed head
o	free stream
1	duct entrance (station 62 for submerged inlet, station 1 for nose inlet)
2	station 86.5
3	station 97
4	station 134
5	station where air discharged from outlet has returned to free-stream static pressure
a,b,c,d	separate measurements at a given station
s	surface

TECHNIQUE AND MODELS

The present investigation was conducted employing the recoverable free-fall-model technique described in reference 16. In this technique

the model is released from a carrier airplane at about 40,000-feet pressure altitude and accelerates in free fall to a Mach number of about 1.10 to 1.15. The speed of the model is then reduced by the extension of an umbrella-type dive brake (shown on a model without inlets in fig. 1). When the speed of the model has been sufficiently reduced, a parachute is ejected from a container aft of the dive brake and the model is lowered to the ground at a speed of less than 50 feet per second.

The models employed in the present tests were a model without inlets (figs. 1 and 2, hereinafter referred to as the basic model), a twin submerged-inlet model (figs. 3 and 4), and a nose-inlet model (figs. 5 and 6). The models were all 211 inches in length (exclusive of nose-boom length) with a fineness ratio of 12.4, and weighed about 1100 pounds. The model fins were oriented for 0° incidence. The screws used to attach the external skin were inserted flush to the skin, but were not filled with any smoothing compound. The hangers used to attach the model to the carrier airplane were retracted into the model, flush with the skin when the model was released. The airspeed head employed on all models is shown in figure 7.

The inlet of the submerged-inlet model (figs. 3 and 4) had a 7° ramp with curved divergent walls (reference 1). Each entry had a cross-sectional area of 13.62 square inches and an aspect ratio of 4. The air-outlet design (fig. 4(c)) was based on the necessity of discharging the air forward of the dive brake.

The inlet of the nose-inlet model (figs. 5 and 6) comprised, in the nomenclature of reference 9, an NACA series I-35.8-600 nose inlet with a 1.5-inch-diameter airspeed boom (fig. 6) projecting from the center. The area of the annulus was equivalent to the sum of the two inlet areas of the submerged-inlet model. The model aft of station 102 was identical to the submerged-inlet model.

It was considered that the size of the inlet models would be most suitable for a drag comparison if the same amount of usable volume were provided in both models. The nose-inlet model, being the same length as the submerged-inlet model, had a greater surface area and volume than the submerged-inlet model. The additional volume, however, was almost entirely consumed by the additional ducting required for the nose inlet.

INSTRUMENTATION AND TESTS

The instruments employed in the models and the carrier airplane, their purpose, ranges, and estimated accuracy are described in reference 16.

The instruments installed in the models consisted of an airspeed and altitude recorder, a sensitive accelerometer for measuring total drag, and recording manometers to measure various pressures. All instruments were compensated for the temperatures experienced within the heated interior of the model.

The locations of the pressure tubes and orifices in the submerged- and nose-inlet models are shown in figures 3 and 5, respectively. The pressure tube and orifice instrumentation common to both inlet models consisted of a total-pressure rake at station 86.5 (fig. 3(c)) for determining the pressure recovery and a total and static pressure rake at station 134 (fig. 3(c)) for pressure measurements required to evaluate the internal drag. Various sonic nozzles were installed in the ducting with sonic throats at station 97 to control and measure the flow through the ducting. Pressure orifices were installed in the throat at station 97 (fig. 3(a)) to check the presence of sonic flow at this station. The duct instrumentation was installed in both ducts for symmetry; however, only that in one duct was used for measurements in the present tests. Orifices were installed along the center line of the ramp and lip surfaces of the submerged inlet to obtain the pressure distribution on these surfaces. A rake was installed at the entrance to the nose inlet (fig. 5(b)) to measure the influence of the nose boom on the pressure recovery at the inlet. On one drop a boundary-layer rake was installed at station 60 of the basic model to measure the characteristics of the boundary layer for correlation with the pressure recovery of the submerged inlet model. (Station 60 is the location of the leading edge of the lip of the submerged inlet model.)

The pressure measuring system was designed to render any effects of lag negligible. For longer lines, such as airspeed-head lines, the tubing was 3/16-inch inside diameter. Shorter tubes were 1/8-inch inside diameter.

Instruments were installed in a temperature-controlled compartment of the carrier airplane to record atmospheric data during the ascent of the airplane and to record the model release conditions. These instruments consisted of airspeed and altitude recorders, a galvanometer and resistance bulb thermometer for measuring atmospheric temperature, and an instrument timer to actuate a common timing circuit.

During the ascent of the carrier airplane atmospheric data were recorded at about 1,000-feet intervals. The airplane was oriented in level flight at about 40,000-feet pressure altitude for the drop run. The airplane and model instruments were placed in operation 10 seconds prior to release to record the release conditions and to assure that the model instrument motors were up to speed at the time of release. After release, the model accelerated to a Mach number of about 1.1. Typical

Reynolds number and Mach number variations during the free fall are given in figure 8.

The tests included two drops of the basic model, one to evaluate the drag of the model and the other to measure boundary-layer characteristics at station 60. Both inlet models were tested with sonic-throat to inlet-area ratios of 0.477, 0.683, 0.777, and 0.889 to determine the drag and pressure recovery of the models over a mass-flow-ratio range of about 0.4 to 0.8. In addition, the submerged-inlet model was tested with a sonic-throat to inlet-area ratio of 0.579.

REDUCTION OF DATA

The static-pressure-error coefficients of the airspeed head (fig. 9) were employed in evaluating free-stream Mach number. Figure 9 was derived from a correlation of data obtained during the model drop with airplane atmospheric-survey data as described in the appendix of reference 16. The internal drag and mass-flow ratio were also evaluated as described in reference 16. The inlet incremental drag for both models and the additive drag for the nose-inlet model were evaluated as described in the appendix.

The total pressures in the ducts, particularly in the case of the nose inlet, fluctuated with time. These fluctuations are believed to be traceable to slight model oscillations during the free fall and the attendant effects on the boundary layer ahead of the inlets. In the case of the boundary layer flowing along the nose boom of the nose inlet, these fluctuations are illustrated by the pressure-recovery measurements at station 1, as shown in figure 10. During the tests of the nose-inlet model at a mass-flow ratio of about 0.4 ($A_8/A_1 = 0.477$), the flow along the nose boom apparently separated at a Mach number of 1.07 and caused fluctuations in the accelerometer reading (drag) and large fluctuations in the duct pressures. Data for this test were reduced up to a Mach number of 1.07 only.

For the data presented, the total-pressure fluctuations were insufficient to affect the drag or mass-flow ratios. Although the total pressure distribution and fluctuations at station 86.5 of both models were small compared to those at the entrance of the nose-inlet model, a faired curve through average values plotted as a function of time was employed to evaluate pressure recovery.

RESULTS

The variation of the external drag coefficient of the basic model with free-stream Mach number is shown in figure 11. The characteristics of the boundary layer at station 60 of the basic model are given in figure 12.

The variation of the drag coefficients, the pressure recovery, and the mass-flow ratio with free-stream Mach number for each test of the submerged- and nose-inlet models is presented in figures 13 and 14, respectively. Drag data for the test of the submerged-inlet model with a sonic-throat to inlet-area ratio of 0.477 were known to be erroneous and are not included in figure 13(e). Local Mach number distributions on the ramp of the submerged inlet at mass-flow ratios about 0.4, 0.6, and 0.8 are shown in figure 15 and the pressure distributions along the lip of the submerged inlet at mass-flow ratios of about 0.5 and 0.7 are given in figure 16.

The variation of the external drag coefficients of the submerged- and nose-inlet models with mass-flow ratio for various Mach numbers is presented in figure 17. Figure 18 shows the external drag coefficients less the inlet incremental drag coefficients at Mach numbers of 0.9 and 1.10 for both models, and the external drag coefficients less the additive drag coefficients for the nose-inlet model.

The variation of the pressure recovery of the submerged- and nose-inlet models with mass-flow ratio at various Mach numbers is shown in figures 19 and 20, respectively. The pressure recovery at the duct entrance shown in these figures was evaluated from the pressure recovery at station 86.5 using duct efficiency factors established by ground tests which are assumed to be valid for the Mach number range of the present tests. Figure 21 shows the variation of the entrance pressure recovery of the submerged inlet with Mach number for various mass-flow ratios.

The maximum pressure recovery of the submerged inlet is compared with results of other investigations in figure 22, and the variation of pressure recovery of the submerged inlet with mass-flow ratio at Mach numbers of 0.8 and 1.10 is compared with previous results in figure 23.

ACCURACY OF RESULTS

Based on the scatter of the experimental data, the maximum errors involved in the evaluation of free-stream Mach number, mass-flow ratio,

and external drag are tabulated below:

Quantity	Estimated maximum error
M_o	±0.02 at a Mach number of 0.75 ±.01 at Mach numbers above 0.85
$\frac{m_1}{m_o}$	±.01
C_{D_E}	±.01 below a Mach number of 1 ±.005 above a Mach number of 1

DISCUSSION OF RESULTS

Drag

A comparison of figure 11 with figures 13 and 14 shows that the Mach number of drag divergence for the inlet models was about the same as that of the basic model.

The external drag of the nose-inlet model was less than that of the submerged-inlet model throughout the test Mach number range as shown in figure 17. The difference in drag coefficient based on the model maximum cross-sectional area was about 0.02 at supersonic speeds and about 0.015 at subsonic speeds. For a hypothetical airplane, with a ratio of fuselage maximum cross-sectional area to wing area of 0.06, the difference in airplane drag coefficient based on wing area would be relatively small, about 0.0012 at supersonic speeds and about 0.0009 at subsonic speeds. If the drag comparison is made after subtracting the inlet incremental drag (discussed in the appendix) as shown in figure 18, the drag difference would remain about the same as that described above.

The above drag comparison is for the submerged-inlet model and the nose-inlet model with the nose boom projecting from the center of the models. The external drag of the nose-inlet model without a nose boom would be essentially the same as that of the model tested. This is based on the fact that changes in mass-flow ratio (which is a factor causing large changes in the entering stream tube) did not have much influence on the external drag in the present tests and also in those of reference 13; consequently, the small changes to the entering stream tube resulting from the presence of the nose boom would have a negligible effect on the external drag. After the inlet incremental drags are subtracted from the external drags ($C_{D_E} - C_{D_a}$) in figure 18, the resulting drag for the nose-inlet model is higher than the drag that would prevail for a model without a boom because it includes the drag of

the nose boom. The drag of the boom is relatively large because of the adverse pressure gradient on the boom. The drag resulting from pressure and viscous forces on the external surface of this model without the nose boom is also evident from figure 18 where the additive drag is subtracted from the external drag ($C_{D_E} - C_{D_A}$). A comparison of the ($C_{D_E} - C_{D_a}$) curve for the submerged-inlet model with the ($C_{D_E} - C_{D_A}$) curve for the nose-inlet model shows that the external surface drag would be about 0.03 to 0.04 less for a nose-inlet model without a boom than the corresponding drag of the submerged-inlet model.

The external drag of both inlet models (fig. 17) increased slightly with increasing mass-flow ratio. This result is in reasonable agreement with that of reference 13 which shows the external drag of a series I nose-inlet model to be practically constant throughout the mass-flow-ratio range of 0.4 to 0.8 at Mach numbers less than 1.2. For an open nose-inlet model, the external drag at subsonic speeds is stated to be constant in reference 17, with the increase in additive drag (inlet incremental drag in the case of an open nose inlet) associated with a decrease in mass-flow ratio being compensated by a corresponding increase in lip leading-edge suction. Since the external drag (fig. 17) decreased slightly as the mass-flow ratio was decreased, it is evident that the pressure drag of the inlet models changed in such a manner as to more than offset the increase in inlet incremental drag. Lip pressure distributions were not obtained for the nose-inlet model. Limited lip pressure distributions were obtained for the submerged-inlet model as shown in figure 16. The suction on the outer surface of the lip (fig. 16) increased with decreasing mass-flow ratio from 0.7 to 0.5. This suction, however, was to a large extent offset by the increase of pressure on the inner surface of the lip which is not included as part of the inlet incremental drag (see appendix). The net effect is small in comparison with the change in inlet incremental drag coefficient over the mass-flow-ratio range from 0.7 to 0.5 (fig. 18).

A comparison of the drag of the basic model with that of the nose-inlet model (fig. 17) shows that the external drag of the basic model was about the same as that of the nose-inlet model at the lower mass-flow ratios. Previous results (reference 10) have shown the drag of a series I nose-inlet model to be less than that of a basic model in the transonic flight range. The present results, however, are reasonable because the air-outlet design employed probably provides higher drag than the outlet at the extreme aft end of the model employed in refer-reference 10.

Ram-Recovery Ratios

The ram-recovery ratio of the submerged-inlet model (fig. 21) was almost constant throughout the Mach number range at a mass-flow ratio of 0.8. At lower mass-flow ratios, the pressure recovery in all cases decreased above a Mach number of about 0.90, the amount of decrease increasing with decreasing mass-flow ratio. The decrease at Mach numbers above 0.90 is probably dependent on the boundary-layer shock-wave interaction on the inlet ramp. The effects of the boundary-layer shock-wave interaction on pressure recovery apparently increase as the pressure gradient ahead of the inlet becomes more adverse with decreasing mass-flow ratio.

The maximum entrance pressure recovery of the submerged inlet (fig. 19) occurred at a mass-flow ratio of about 0.6 for the free-stream Mach number range of 0.8 to 1.05. Above a Mach number of 1.05, the pressure recovery was almost constant for mass-flow ratios above 0.6. The maximum pressure recovery is compared with previous results in figure 22 wherein the boundary-layer parameter h/d has been plotted with respect to the maximum pressure recovery for previous results as well as the present results. It is noted that the curve based on the equation

$$\frac{H_1 - p_0}{H_0 - p_0} = 1 - \frac{h}{d}$$

provides reasonable agreement with previous results. The maximum pressure recovery predicted by the curve of figure 22 agrees well with the present results when supersonic speeds did not prevail along the inlet ramp (i.e., at free-stream Mach numbers of 0.9 and below as shown in fig. 15). The decrease in the maximum pressure recovery of the present results is shown in figure 22 to be about 0.035 between a Mach number of 0.90 and 1.10, which is the order of decrease expected on the basis of the total-pressure loss through a normal shock at the maximum local ramp Mach numbers of figure 15.

The variation of the pressure recovery with mass-flow ratio of the submerged-inlet model is compared with previous results in figure 23 at free-stream Mach numbers of 0.80 and 1.10. At a Mach number of 0.80, the boundary-layer parameter h/d of the present tests is nearly equal to those of the previous data and the agreement of the previous pressure-recovery results with the present flight data is considered good. At a Mach number of 1.10, the variation of pressure recovery with mass-flow ratio of the previous data, obtained on a transonic bump, is about the same as that of the present results. The difference in pressure recovery is about 0.075, which can be primarily accounted for by the difference of 0.055 in the boundary-layer parameter h/d between the two sets of data.

The pressure recovery of the nose-inlet model at the duct entrance (fig. 20) increased with increasing mass-flow ratio. This is a result of decreasing losses in the boundary-layer air flowing along the nose boom into the inlet as is indicated by a comparison of figure 10(a) with figure 10(b). These low pressure recoveries for the nose inlet would not prevail in the case of a nose inlet without an airspeed boom projecting ahead of it.

CONCLUSIONS

The following conclusions are based upon the results of an investigation of the drag and pressure recovery of a submerged- and a nose-inlet model in the transonic range. The investigation was conducted for a mass-flow-ratio range of about 0.4 to 0.8 over a Mach number range of about 0.8 to 1.10.

1. The Mach number of drag divergence of the inlet models was about the same as that of a basic model without inlets.

2. For a given mass-flow ratio, the external drag of the nose-inlet model was less than that of the submerged-inlet model; about 0.02 (based on maximum model cross-sectional area) less at supersonic speeds and about 0.015 less at subsonic speeds.

3. The maximum pressure recovery of the submerged inlet model, at subsonic speeds, agreed well with the value predicted from previous subsonic data. When supersonic speeds prevailed on the inlet ramp, the maximum pressure recovery decreased approximately the amount anticipated for the total-pressure loss through a normal shock at the maximum local Mach number on the ramp.

4. The variation of pressure recovery of the submerged inlet with mass-flow ratio at subsonic speeds and supersonic speeds is in reasonable agreement with previous wind-tunnel results.

Ames Aeronautical Laboratory,
National Advisory Committee for Aeronautics,
Moffett Field, Calif.

APPENDIX

INTERNAL, INLET INCREMENTAL, AND ADDITIVE DRAG

Internal drag has been defined in various manners based on momentum considerations of the internal flow. The various internal drag concepts and their applications in the present report are discussed below.

Consider the two-dimensional model illustrated in figure 24(a). The model is assumed to be at 0° angle of attack, the inlet and outlet areas are considered normal to the free stream, and the velocities of the flow at stations 1 and 4 are assumed uniform and parallel to the free stream. The following considerations differentiate between the actual pressure plus viscous drag forces occurring within a duct interior (stations 1 to 4 of fig. 24(a)) and the quantity normally called internal drag which considers the viscous losses and pressure forces in the drag direction associated with the internal flow from free-stream conditions (station 0) to the exit (station 4) or to a station aft of the exit where free-stream static pressure prevails (station 5). The difference between the pressure plus viscous force within the duct interior and the internal drag (as just defined) gives rise to such concepts as scoop incremental drag (reference 18), and additive drag in the case of an open nose inlet (reference 19).

Friction and Pressure Drag Within a Duct

The actual friction plus pressure drag experienced within the duct may be expressed by momentum considerations of the flow between the inlet and the exit. The momentum equation may be written

$$p_1 A_1 + m V_1 - \int_1^4 p \, dA_x - (D_f)_{1-4} = p_4 A_4 + m V_4 \qquad (1)$$

where $(D_f)_{1-4}$ is the momentum loss resulting from friction. In order to refer the pressures to free-stream static pressure, the equation

$$p_0 A_1 - \int_1^4 p_0 \, dA_x = p_0 A_4 \qquad (2)$$

is subtracted from equation (1) to provide the following relationship:

$$\int_1^4 (p - p_o)\, dA_x + (D_f)_{1-4} = m(V_1 - V_4) + (p_1 - p_o) A_1 - (p_4 - p_o) A_4 \qquad (3)$$

which provides the pressure plus friction drag within the duct interior.

Internal Drag

The quantity normally called internal drag is the pressure forces in the drag direction and the viscous losses associated with the internal flow from free-stream conditions ahead of the model to a region aft of the model where free-stream static pressure prevails. Because of the general acceptance of this definition of internal drag, this designation is employed in the present report. Applying the momentum equations between stations 0 and 5, in a manner similar to that employed to obtain equation (3), results in the expression

$$D_I = \int_0^5 (p - p_o)\, dA_x + (D_f)_{0-5} = m\,(V_o - V_5) \qquad (4)$$

where dA_x is the incremental surface component normal to the free stream of the model surfaces and the stream tube bounding the internal flow. The quantity $(D_f)_{0-4}$ is normally employed instead of $(D_f)_{0-5}$ because V_5 is evaluated from conditions at the exit assuming no losses in total pressure between stations 4 and 5.

Another expression for internal drag that has been used is based on momentum considerations between free stream and the exit or

$$(D_I)' = \int_0^4 (p - p_o)\, dA_x + (D_f)_{0-4} = m\,(V_o - V_4) - (p_4 - p_o) A_4 \qquad (5)$$

Equations (4) and (5) are not equivalent, although they generally yield equivalent results because the static pressure at the exit is near free-stream static pressure. In the case of the present investigation, these equations yielded practically identical results.

Inlet Incremental Drag

The difference between the pressure plus viscous drag within the ducting and the internal drag (equation (4) or (5)) is large at reduced mass-flow ratios, particularly at supersonic speeds. This difference

(strictly, the difference between equations (3) and (5)) is defined as inlet incremental drag herein and may be expressed as

$$D_a = -\int_o^1 (p - p_o)dA_x - (D_f)_{o-1} = m(V_1 - V_o) + (p_1 - p_o)\,A_1 \qquad (6)$$

The quantity D_a is identical to the scoop incremental drag of reference 18, which is defined as the sum of the pressure forces (in the drag direction) on the entering stream tube including the pressure forces on the stream tube adjacent to the body and the friction losses of the stream prior to entry into the duct. Thus, when the drag of all components external to the duct is desired (equation (3)), or the sum of the inlet incremental drag (equation (6)) and the internal drag (equation (4) or (5)), must be subtracted from the total drag. The inlet incremental drag coefficient, based on equation (6), may be expressed as a function of pressure recovery and mass-flow ratio at a given Mach number (reference 18).

Additive Drag

In the case of an open nose inlet, equation (6) is also equivalent to the quantity called additive drag in reference 19, which may be defined as the sum of the pressure forces (in the drag direction) on the stream tube prior to entry into the duct not including the pressure forces on the part of the stream tube adjacent to the body surface. Additive drag may in the general case (with reference to fig. 24(a)) be expressed mathematically as

$$D_A = \int_o^1 (p - p_o)\,(d\,A_x)_{S.T.} \qquad (7)$$

where $(dA_x)_{S.T.}$ is the incremental component of area normal to the free stream of the stream tube not including the forces on the stream tube adjacent to the body surface. Additive drag, instead of inlet incremental drag, is subtracted from the external drag when the resulting external pressure plus viscous drag is not to include the drag of the surfaces of the body adjacent to the internal flow.

Application of Equation (6) to Rounded Lip

The application of equation (6) requires that the area A_1 be defined. In the case of a sharp lip (fig. 24(b)), the stagnation point

is generally at the lip leading edge and the area A_1 is known. In the case of a rounded lip (fig. 24(b)), however, the location of the stagnation point is not generally known and the area A_1 is generally unknown.

In the case of a rounded lip, it is convenient to employ the duct area aft of the rounded portion of the lip (station 1 of fig. 24(b)) as the area A_1. This, of course, means that the pressure and friction forces on the duct and lip ahead of station 1 are considered part of the external surface drag ($C_{D_E} - C_{D_a}$). By doing this, however, the computations are simplified because the inlet area employed is that upon which the mass-flow ratio is conventionally based and the inlet incremental drag becomes independent of lip shape at a given mass-flow ratio and pressure recovery for a given free-stream Mach number.

Evaluation of Drags for Inlets of This Report

The external drag coefficient was evaluated, as described in reference 16, by subtracting the internal drag coefficient (based on the internal drag evaluated from equation (4)) from the total drag coefficient. The drag of all components of the model external to the duct ($C_{D_E} - C_{D_a}$) was evaluated by subtracting the inlet incremental drag coefficient (based on the inlet incremental drag computed from equation (6)) from the external drag. The quantity ($C_{D_E} - C_{D_a}$) includes the drag of the nose boom of the nose-inlet model. In order to evaluate the drag of the external surfaces, not including the nose boom, the additive drag was also evaluated for this model and subtracted, in coefficient form, from the model external drag coefficient. The additive drag was evaluated by assuming that the pressure forces on the external boundaries of the entering stream tube were not affected by the presence of the nose boom. Thus, by assuming a total-pressure recovery of unity at the entrance, and employing equation (6), the additive drag was simply evaluated for various mass-flow ratios. The area employed in equation (6) in this case included the cross-sectional area of the nose boom.

REFERENCES

1. Mossman, Emmet A., and Randall, Lauros M.: An Experimental Investigation of the Design Variables for NACA Submerged Entrances. NACA RM A7I30, 1948.

2. Martin, Norman J., and Holzhauser, Curt A.: An Experimental Investigation at Large Scale of Several Configurations of an NACA Submerged Air Intake. NACA RM A8F21, 1948.

3. Delany, Noel K.: An Investigation of Submerged Air Inlets on a 1/4-Scale Model of a Typical Fighter-Type Airplane. NACA RM A8A20, 1948.

4. Hall, Charles F., and Frank, Joseph L.: Ram-Recovery Characteristics of NACA Submerged Inlets at High Subsonic Speeds. NACA RM A8I29, 1948.

5. Frank, Joseph L.: Pressure-Distribution and Ram-Recovery Characteristics of NACA Submerged Inlets at High Subsonic Speeds. NACA RM A50E02, 1950.

6. Mossman, Emmet A.: A Comparison of Two Submerged Inlets at Subsonic and Transonic Speeds. NACA RM A9F16, 1949.

7. Axelson, John A., and Taylor, Robert A.: Preliminary Investigation of the Transonic Characteristics of an NACA Submerged Inlet. NACA RM A50C13, 1950.

8. Rolls, L. Stewart, and Rathert, George A., Jr.: Tests of a Small-Scale NACA Submerged Inlet at Transonic Mach Numbers. NACA RM A9L29, 1950.

9. Baals, Donald D., Smith, Norman F., and Wright, John B.: The Development and Application of High-Critical-Speed Nose Inlets. NACA Rep. 920, 1948. (Formerly NACA ACR L5F3a)

10. Pendly, Robert E., and Smith, Norman F.: An Investigation of the Characteristics of Three NACA I-Series Nose Inlets at Subcritical and Supercritical Mach Numbers. NACA RM L8L06, 1949.

11. Becker, John V.: Wind-Tunnel Tests of Air Inlet and Outlet Openings on a Streamline Body. NACA ACR, Nov. 1940.

12. Becker, John V., and Baals, Donald D.: High-Speed Tests of a Ducted Body with Various Air-Outlet Openings. NACA ACR, May 1942.

13. Sears, R. I., and Merlet, C. F.: Flight Determination of the Drag and Pressure Recovery of an NACA 1-40-250 Nose Inlet at Mach Numbers from 0.9 to 1.8. NACA RM L50L18, 1951.

14. Brajnikoff, George B., and Rogers, Arthur W.: Characteristics of Four Nose Inlets as Measured at Mach Numbers Between 1.4 and 2.0. NACA RM A51C12, 1951.

15. Wyatt, DeMarquis D., and Hunczak, Henry R.: An Investigation of Convergent-Divergent Diffusers at Mach Number 1.85. NACA RM E50K07, 1951.

16. Selna, James: Preliminary Investigation of a Submerged Inlet and a Nose Inlet in the Transonic Flight Range With Free-Fall Models. NACA RM A51B14, 1951.

17. Fraenkel, L. E.: The External Drag of Some Pitot-Type Intakes at Supersonic Speeds, Part I. Rep. No. Aero 2380, R.A.E. (British), 1950.

18. Klein, Harold: The Calculation of the Scoop Drag for a General Configuration in a Supersonic Stream. Douglas Aircraft Co. Report SM-13744, 1950.

19. Sibulkin, Merwin: Theoretical and Experimental Investigation of Additive Drag. NACA RM E51B13, 1951.

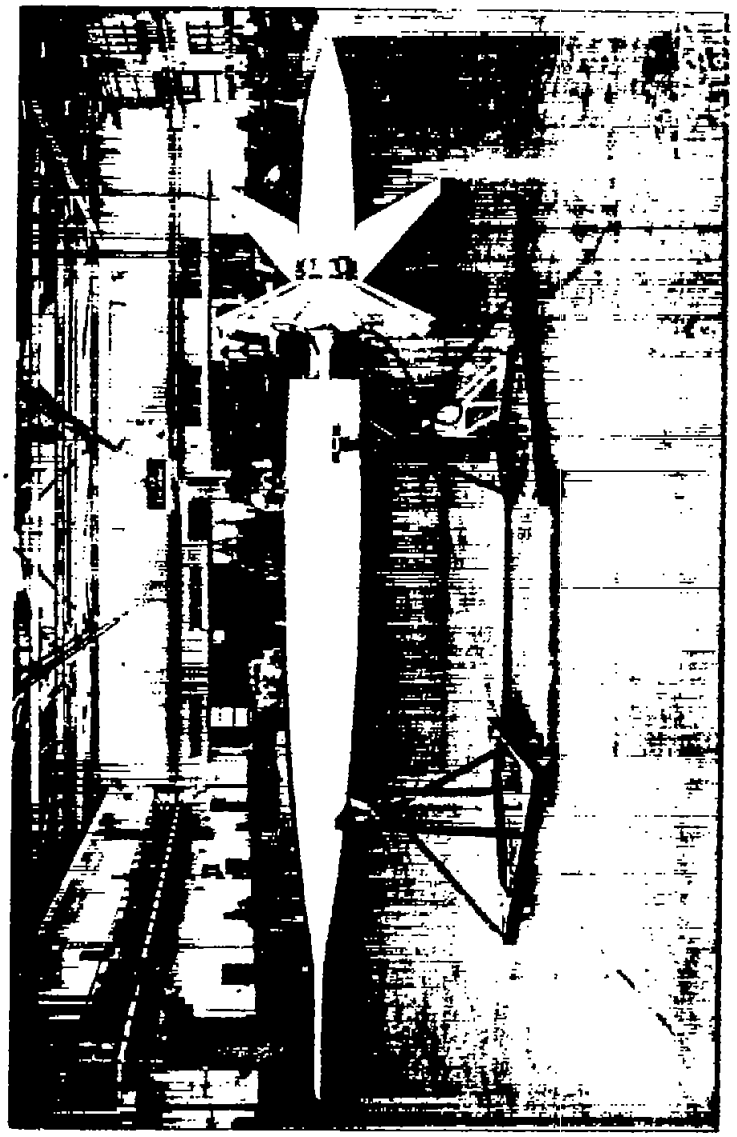

Figure 1.- Basic model with recovery brake extended.

Table of Ordinates		
Station, inches	Outside radius, inches	
	R_1	R_2
0	1.19	- -
5.00	1.70	- -
10.00	2.43	- -
15.00	3.21	- -
20.00	3.90	- -
30.00	5.07	- -
40.00	6.02	- -
50.00	6.78	- -
60.00	7.39	- -
70.00	7.87	- -
80.00	8.20	- -
90.00	8.41	- -
100.00	8.49	- -
102.00	8.50	8.50
110.00	8.46	8.50
120.00	8.30	8.50
130.00	8.02	8.50
135.75	7.79	8.50
146.63	7.25	7.55
150.00	7.07	7.25
154.88	6.82	6.82
160.00	6.56	- -
170.00	6.07	- -
180.00	5.59	- -
192.63	4.89	- -
201.63	3.20	- -
211.00	0	- -

Specifications
Horizontal-tail area (incl 1.30 ft² of fus.) 3.45 ft²
Vertical-tail area (incl 1.30 ft² of fus.) 3.45 ft²
Modal weight, 1057 lb
Center of gravity sta. 86.25
External wetted area (excluding fins) 8515 in.²

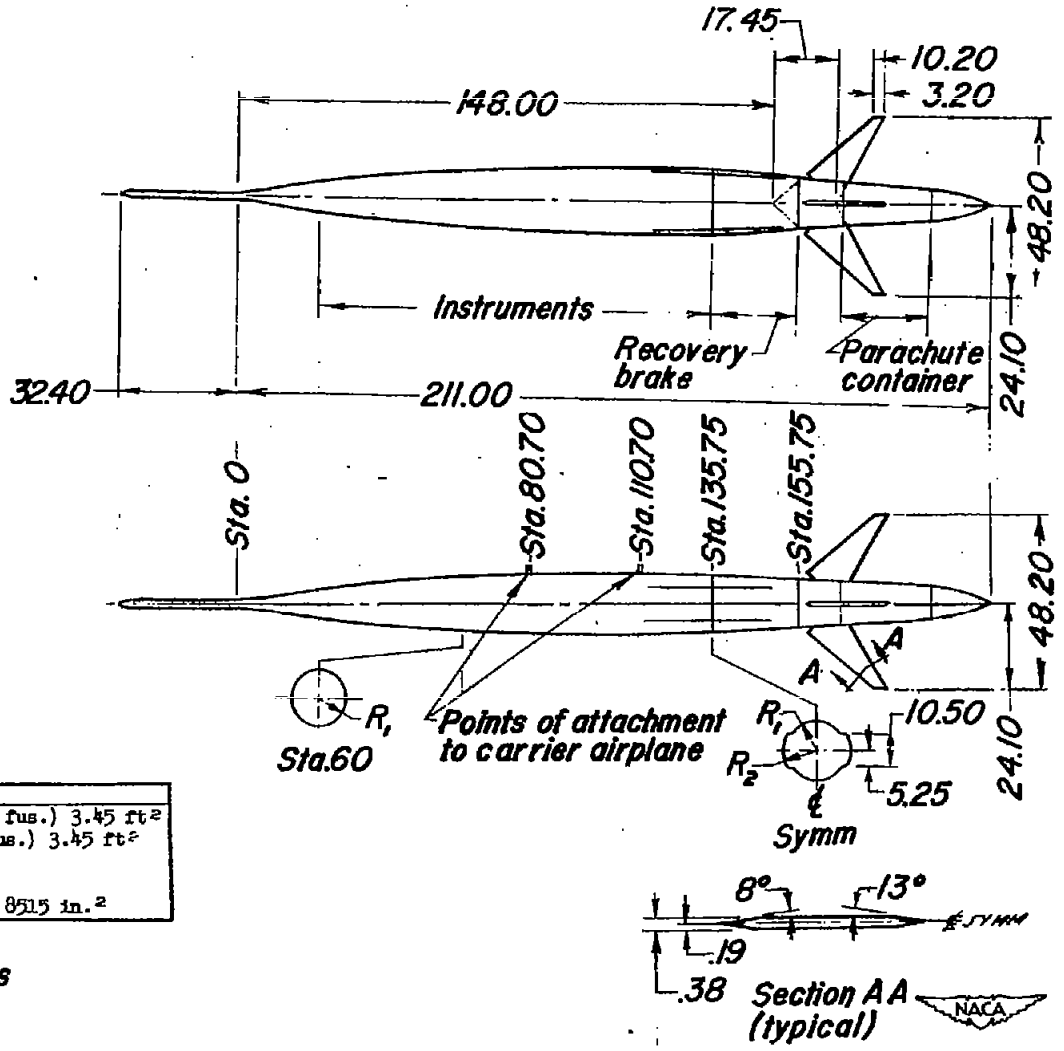

All dimensions are in inches

Figure 2.- Details of basic model.

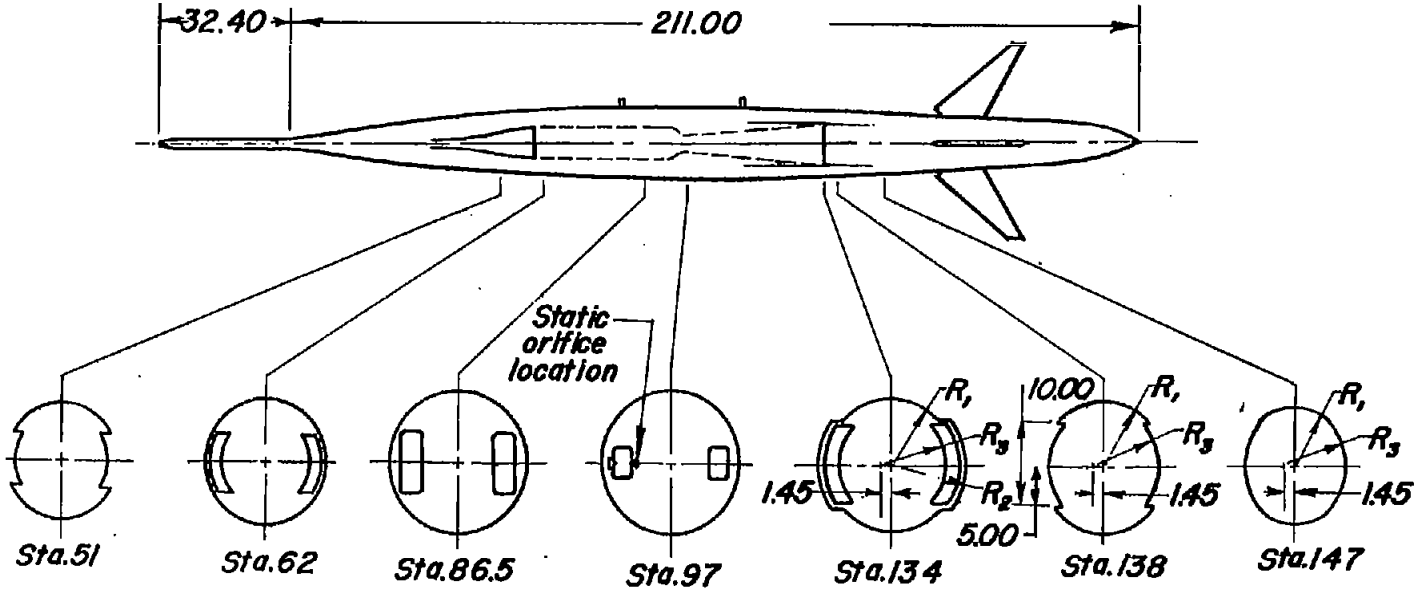

Areas (per duct)
Entrance 13.62 in.^{2} (sta.62)
16.89 in.^{2} (sta. 86.5)
Entrance to throat 17.34 in.^{2} (sta.90)
Outlet 13.75 in.^{2} (sta.135.75)

Specifications
Center of gravity, approximately sta.94
Model weight, approximately 1130 lb.
External wetted area (excluding fins) 8,575 in.^{2}

Note

1. All dimensions are in inches
2. For ordinates of fuselage see figure 2

Exit Dimensions			
Sta.	R_1	R_2	R_3
134.00	7.79	8.50	8.22
138.00	7.68	--	8.22
147.00	7.21	--	8.22

(a) Complete model.

Figure 3.– Details of submerged inlet model.

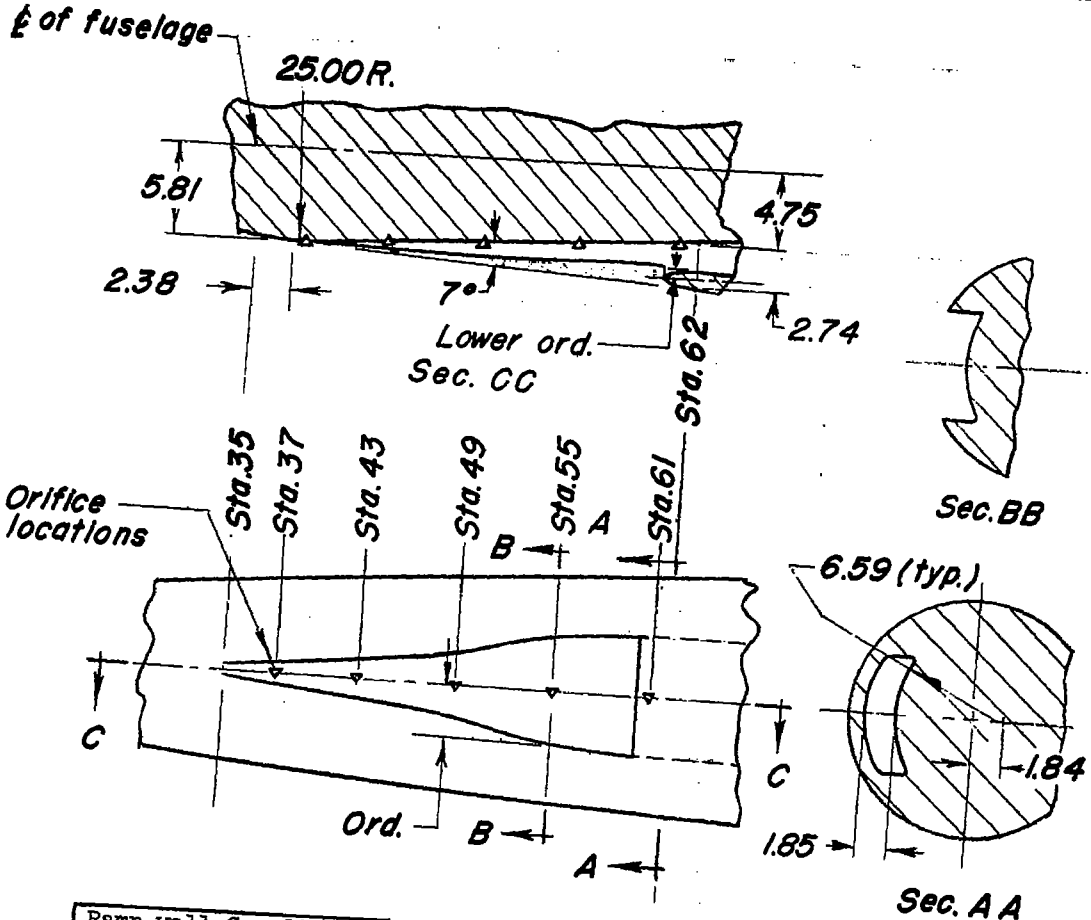

Ramp-wall Coordinates	
Sta.	Ordinates
35.00	0.31
37.50	.59
40.00	.87
42.50	1.16
45.00	1.44
47.50	1.72
50.00	2.27
52.50	2.82
55.00	3.37
57.50	3.67
60.00	3.69
62.00	3.69

Lip Ordinates		
Sta.	Upper ord.	Lower ord.
60.00	0	0
60.25	.22	.23
60.50	.31	.30
60.75	.37	.35
61.00	.42	.38
61.38	.48	.40
62.00	.51	.39
L.E. radius = 0.17		

Note
All dimensions are in inches

(b) Submerged inlet.
Figure 3.- Continued.

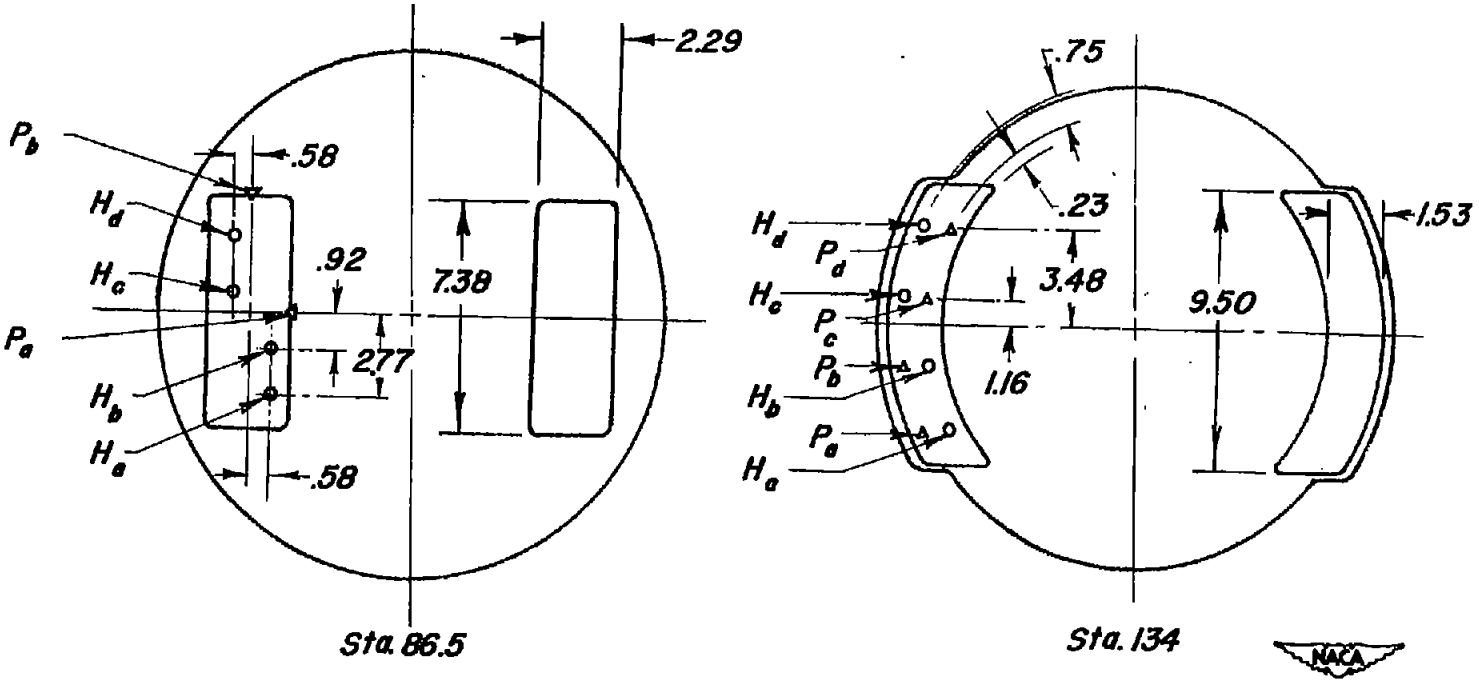

Note
1. H-Total pressure probes
2. P-Static pressure probes
3. All dimensions are in inches

(c) Location of pressure probes and orifices at stations 86.5 and 134.
Figure 3.- Concluded.

(a) Model.

Figure 4.- Submerged inlet model.

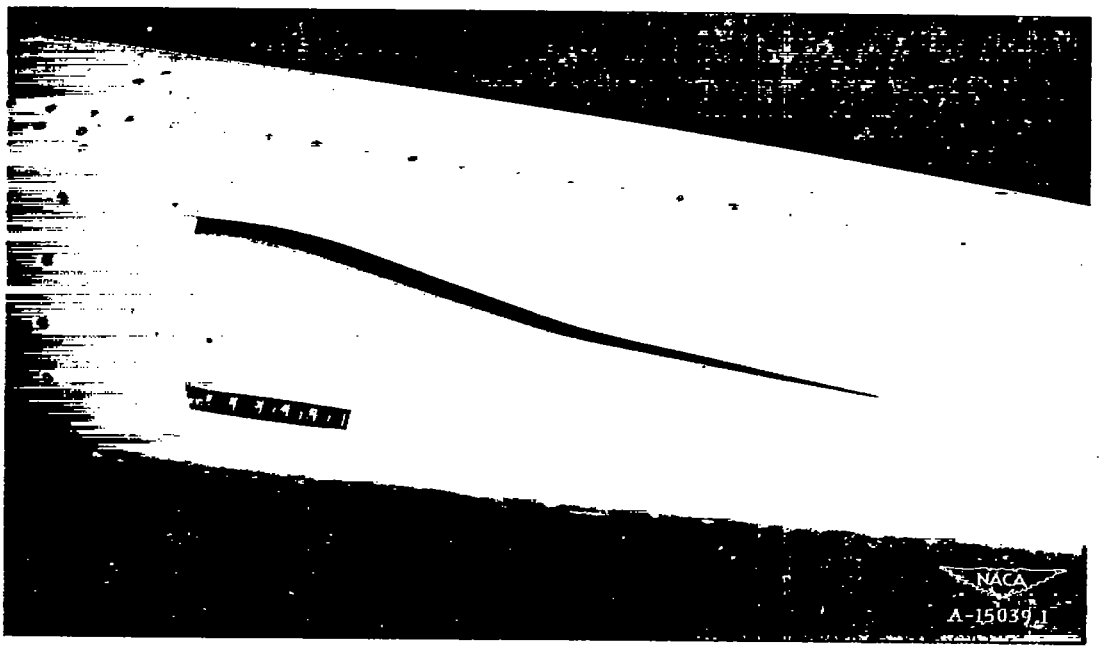

(b) Inlet.

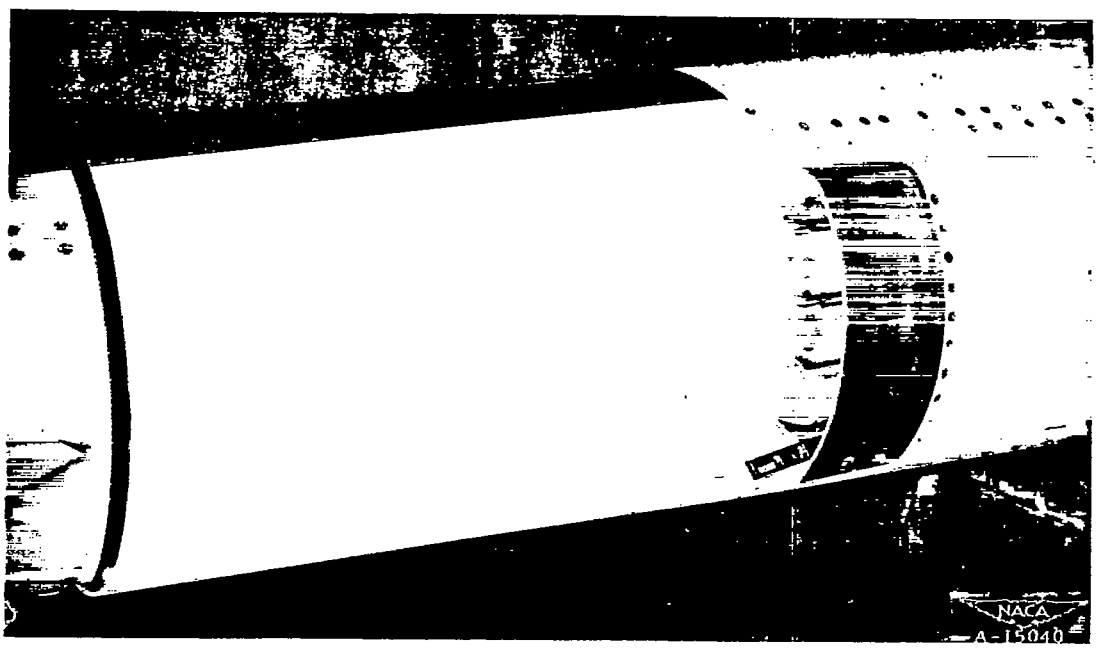

(c) Outlet.

Figure 4.- Concluded.

Table of Ordinates		
Sta.	R_1	R_2
0	3.17	3.17
.20	3.43	3.04
.41	3.53	3.04
.61	3.61	3.04
.82	3.67	3.04
1.53	3.85	3.04
2.55	4.06	3.04
5.00	4.46	3.06
8.16	4.87	3.31
10.20	5.10	3.49
14.28	5.50	3.88
20.40	5.98	4.66
24.48	6.26	5.18
27.00	6.42	5.48
30.00	6.60	- -
40.80	7.16	- -
49.98	7.54	- -
61.20	7.92	- -
70.00	8.15	- -
79.56	8.33	- -
91.80	8.47	- -
102.00	8.50	- -

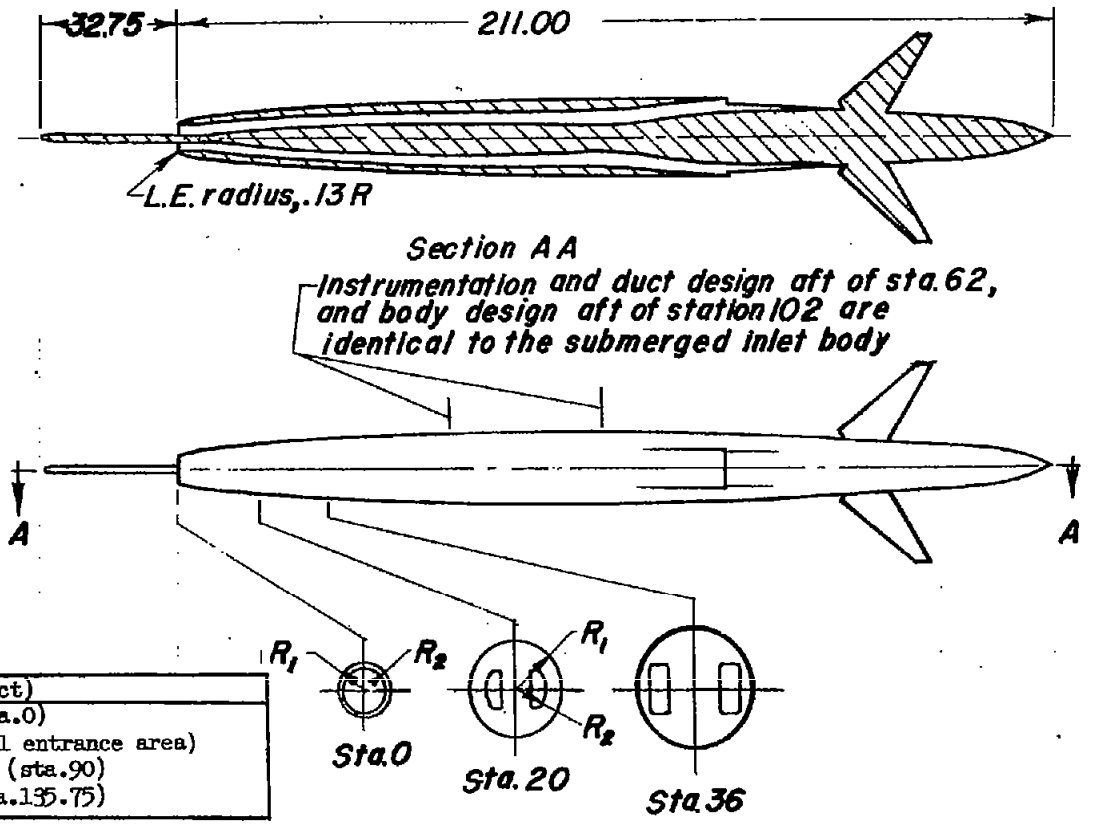

Areas (Per duct)	
Entrance	13.62 in.^{2} (sta.0) (one-half total entrance area)
Entrance to throat	17.34 in.^{2} (sta.90)
Outlet	13.75 in.^{2} (sta.135.75)

Specifications
Model weight, approximately 1070 lb.
Center of gravity, approximately sta.91
External wetted area (excluding fins) 9,124. in.^{2}

Note
All dimensions are in inches

NACA

(a) Complete model.

Figure 5.- Details of NACA series I nose inlet model.

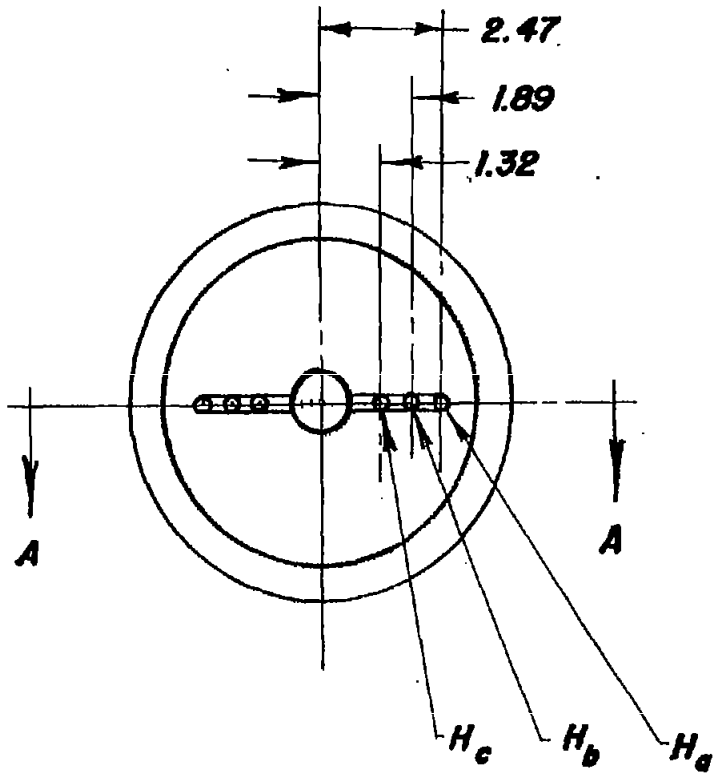

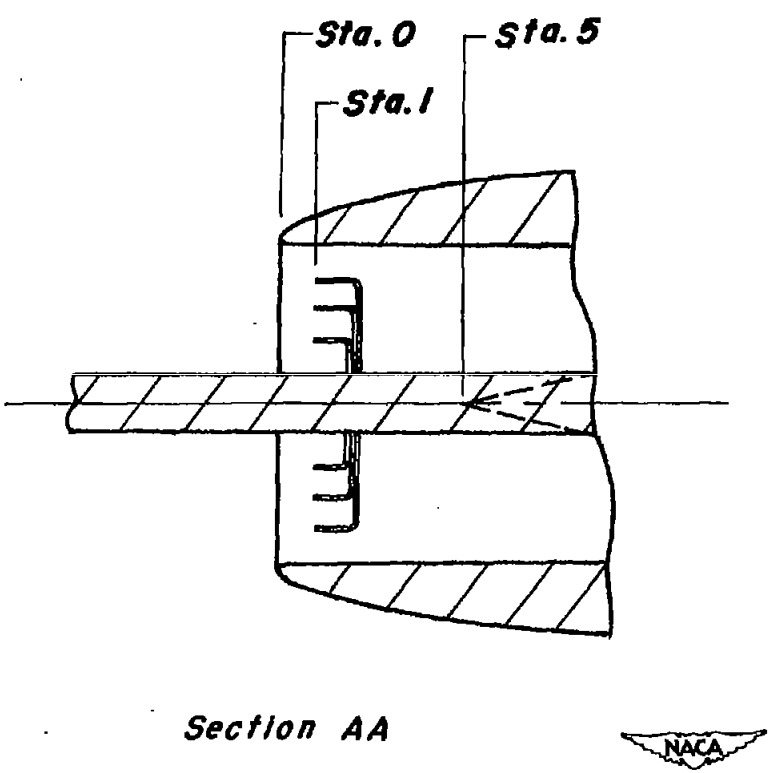

Section AA

Note
All dimensions are in inches

(b) Pressure probes at station 1.

Figure 5.- Concluded.

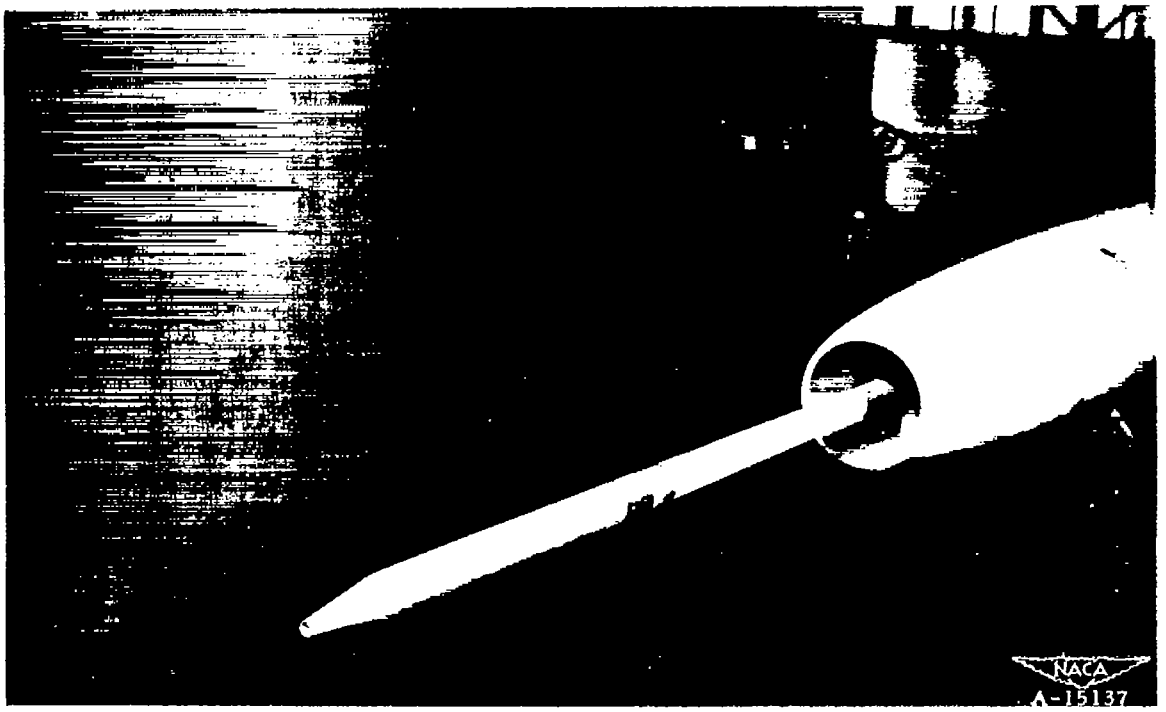

Figure 6.- Nose inlet and airspeed boom installation.

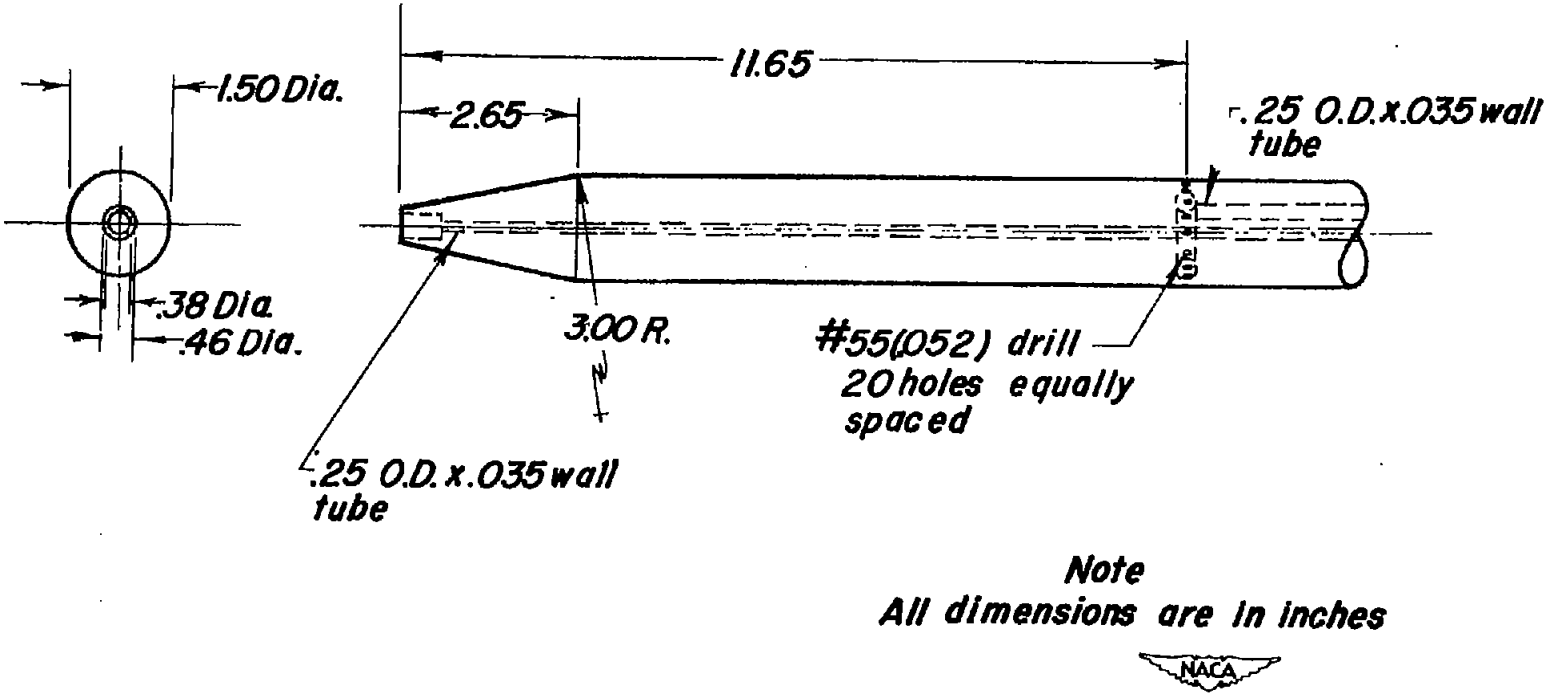

Figure 7.-Airspeed head.

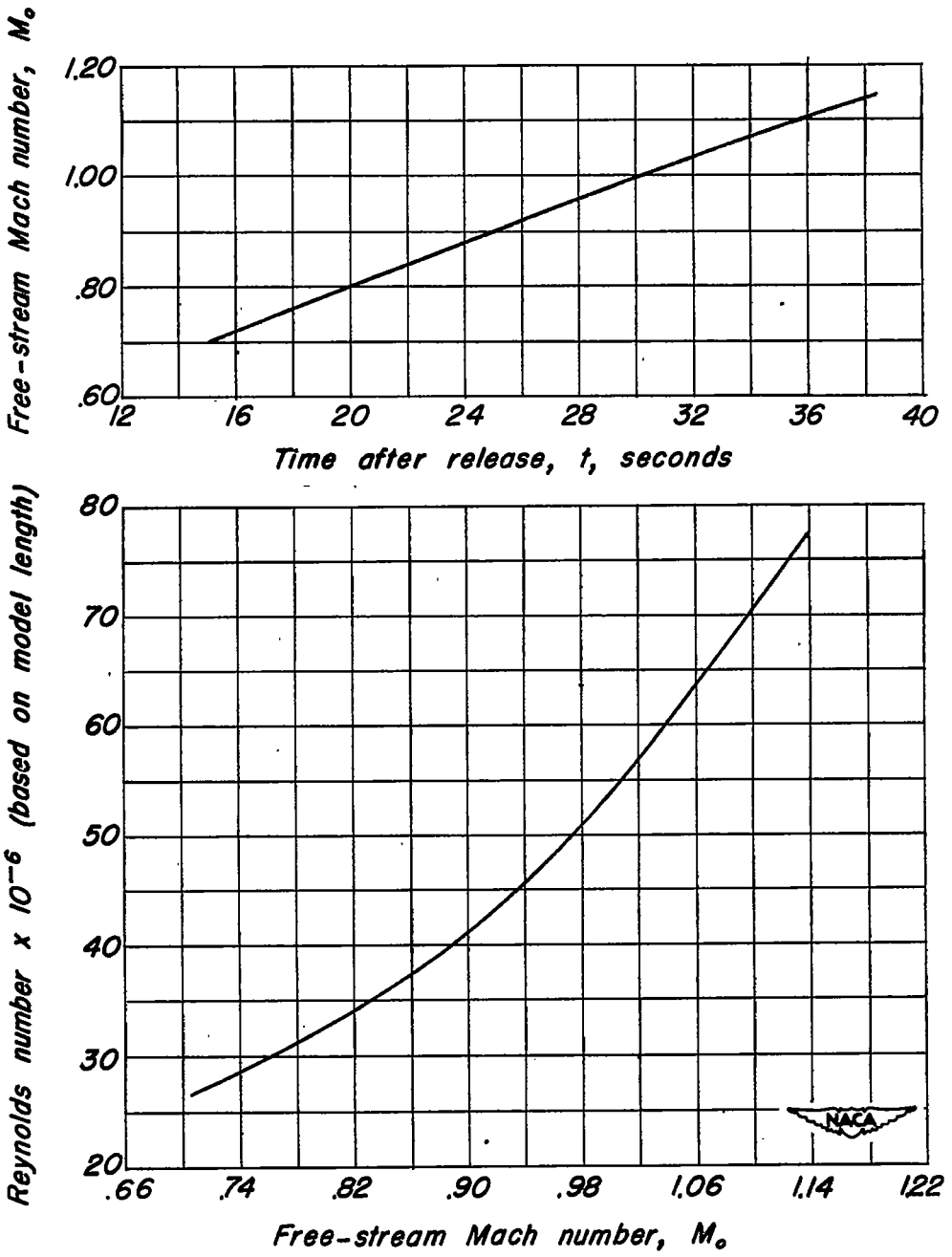

Figure 8.- Typical variation of Mach number with time and Reynolds number with Mach number during free fall of model.

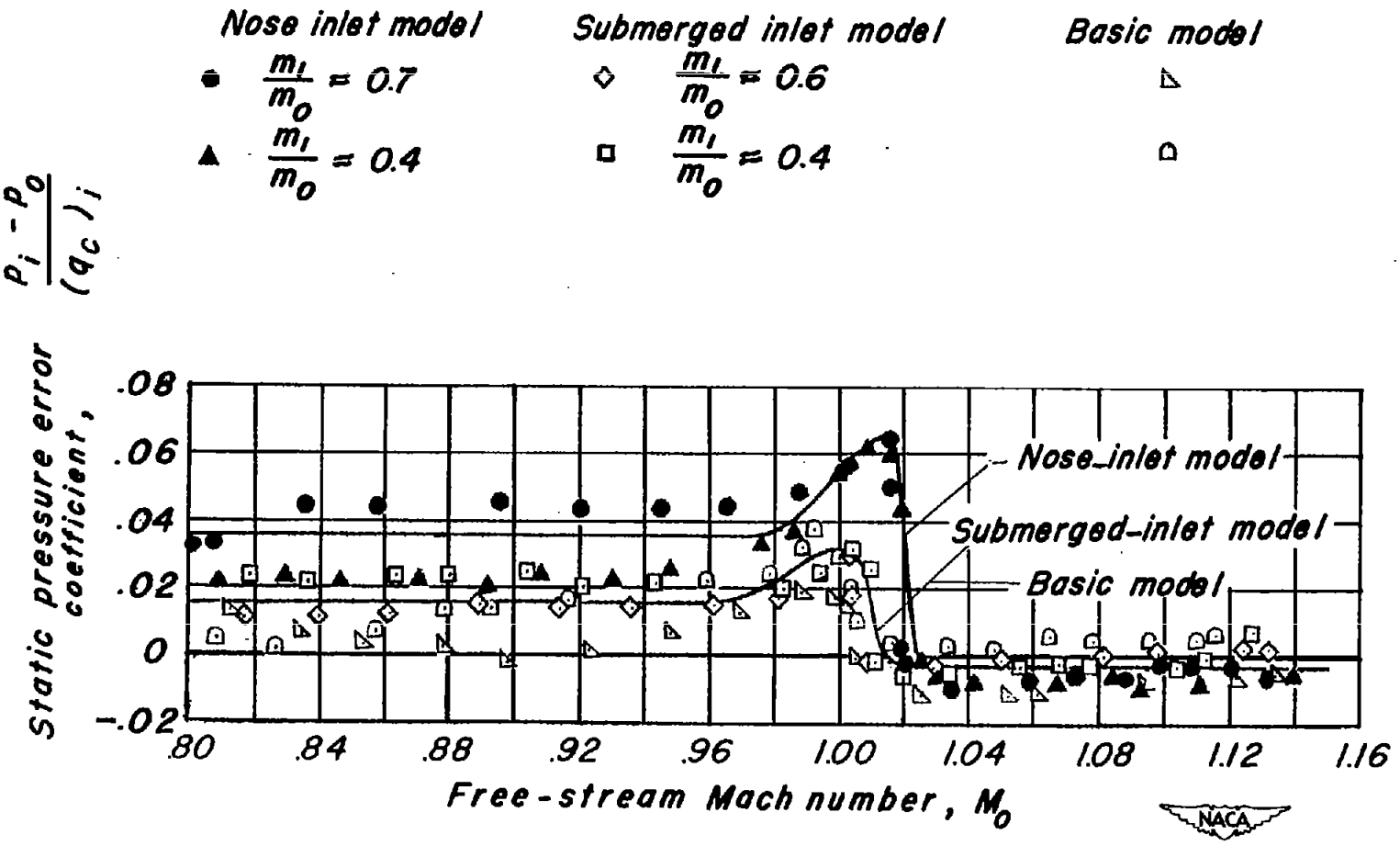

Figure 9. — Variation of static pressure error coefficient with Mach number for the airspeed head.

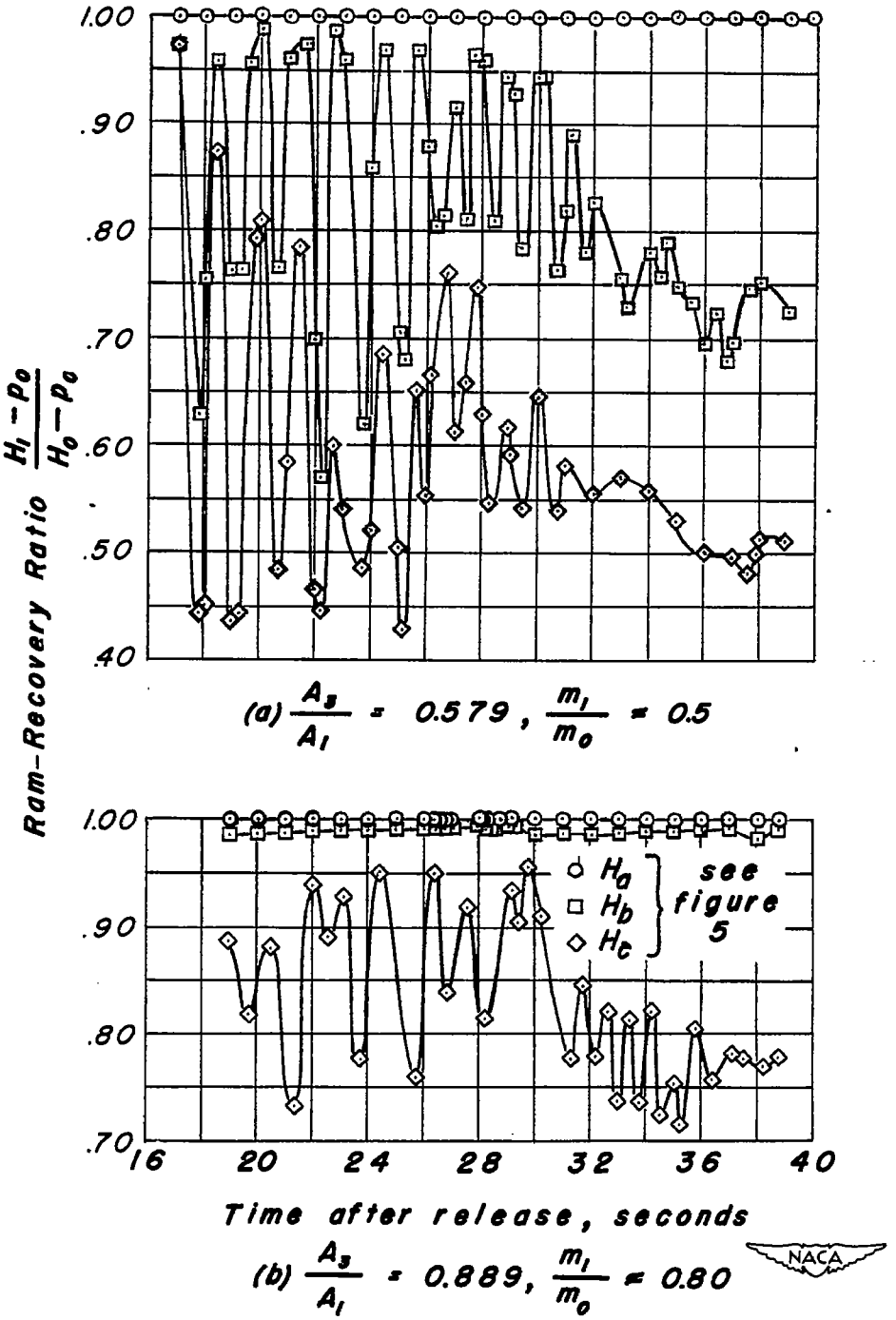

Figure 10.— Pressure—recovery measurements at entrance to nose inlet.

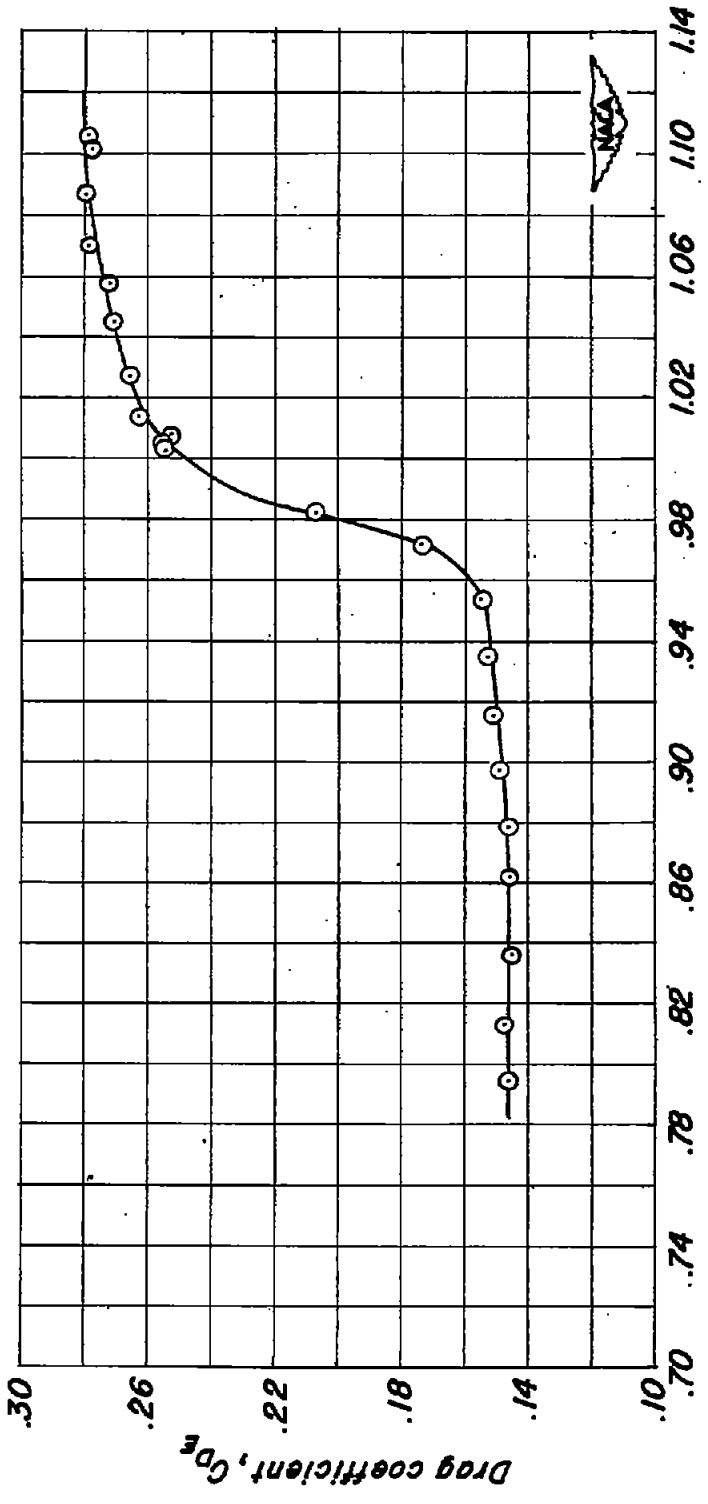

Figure 11.- Variation of drag coefficient of basic model with Mach number.

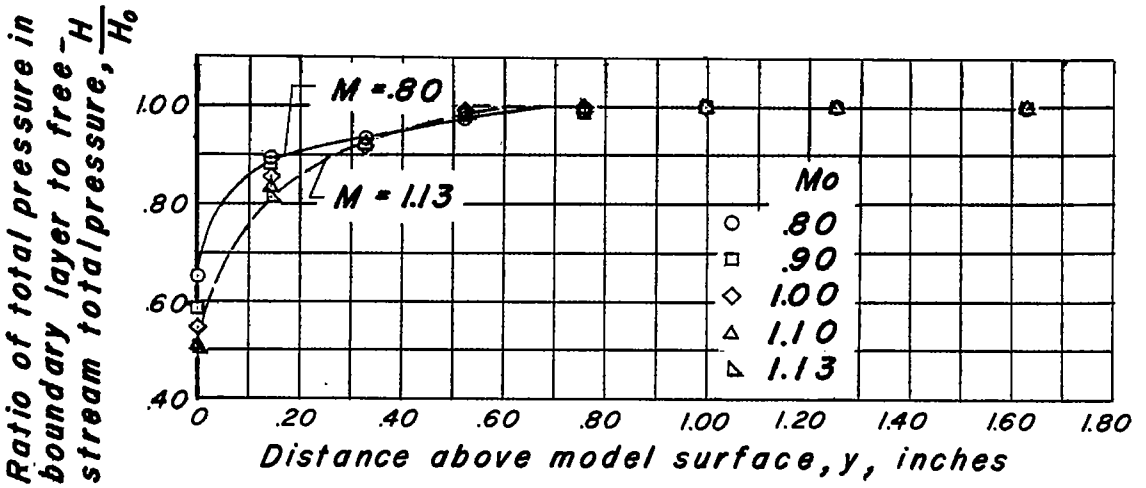

(a) Total-pressure distribution in the boundary layer at various Mach numbers.

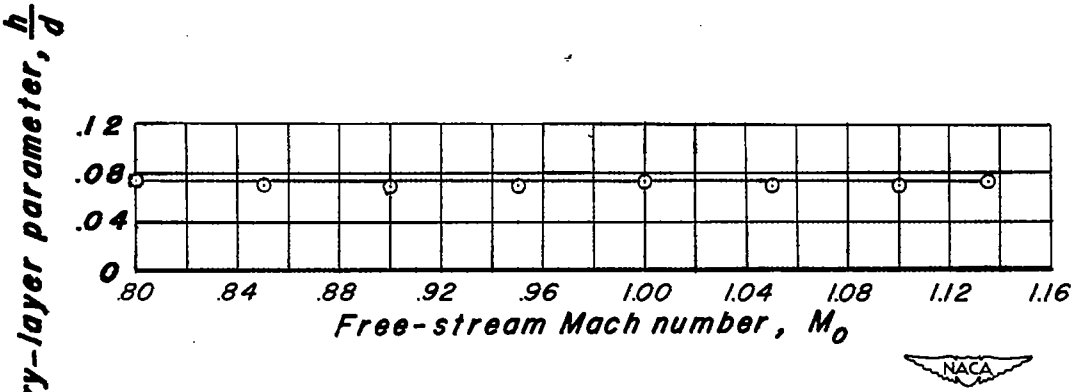

(b) Variation of boundary-layer parameter $\frac{h}{d}$ with free-stream Mach number.

Figure 12. — Boundary-layer characteristics measured at station 60 of the basic model.

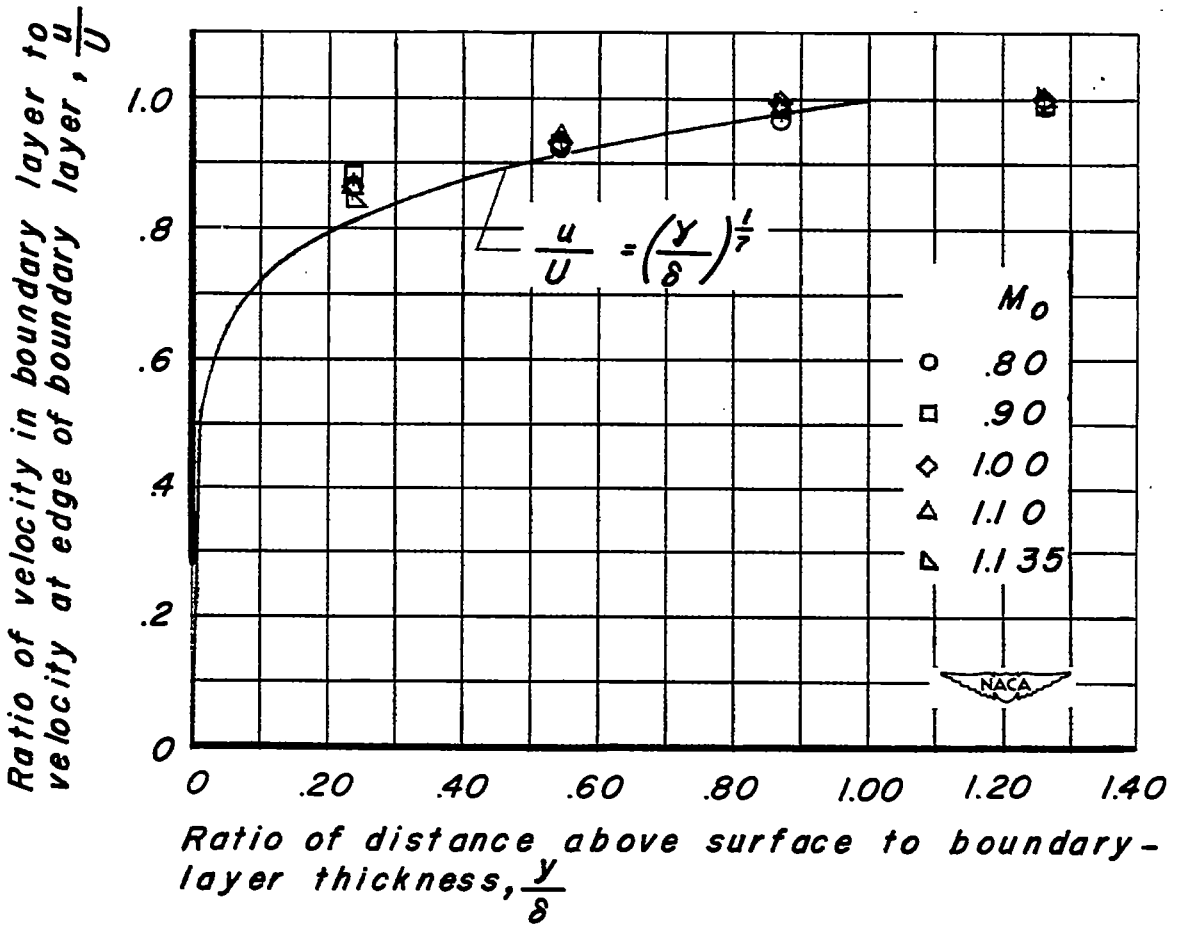

(c) Velocity distribution in boundary layer, $\delta = 0.6$ inches.

Figure 12. — Concluded.

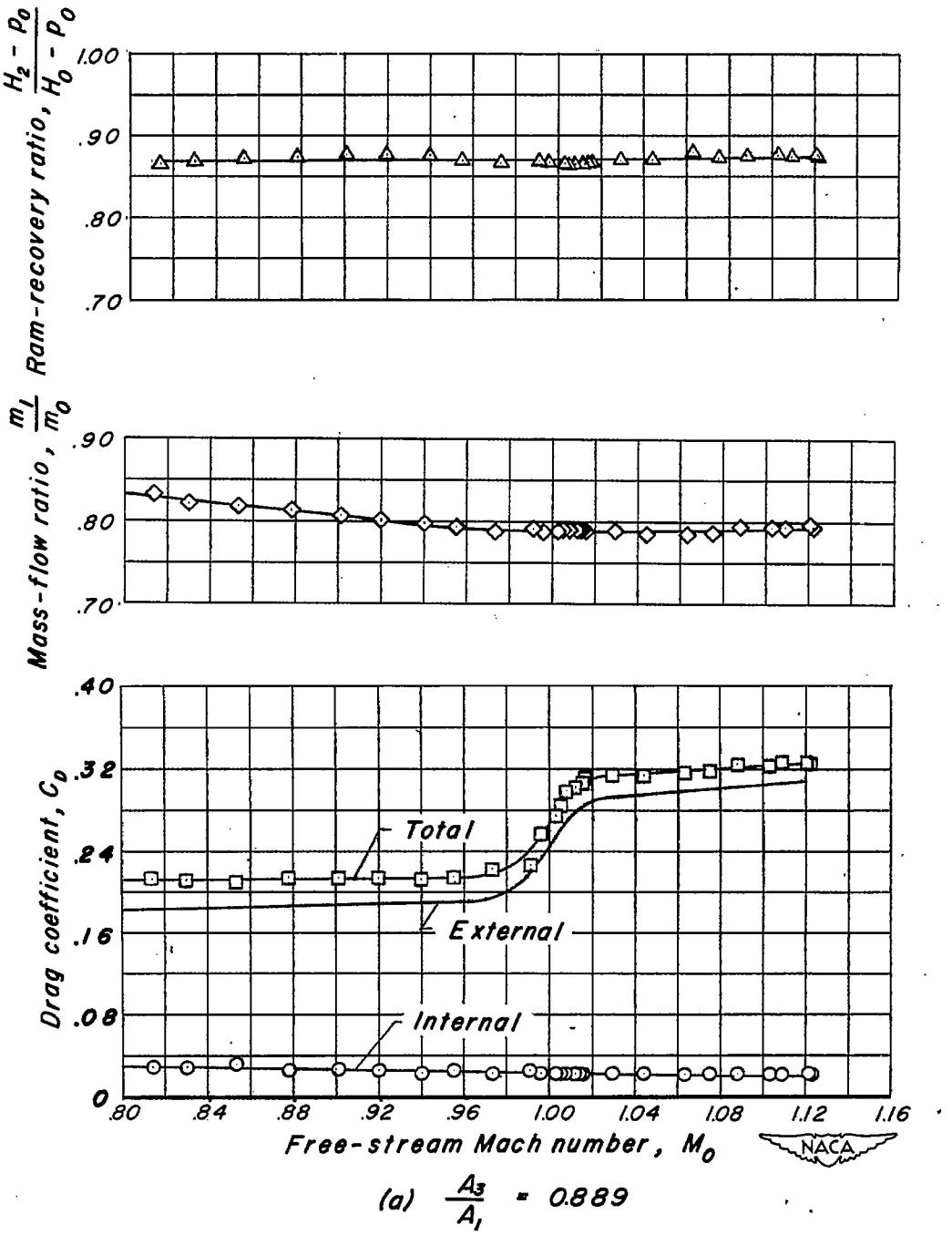

Figure 13. — Variation of drag coefficients, pressure recovery, and mass-flow ratio with free-stream Mach number for submerged inlet model.

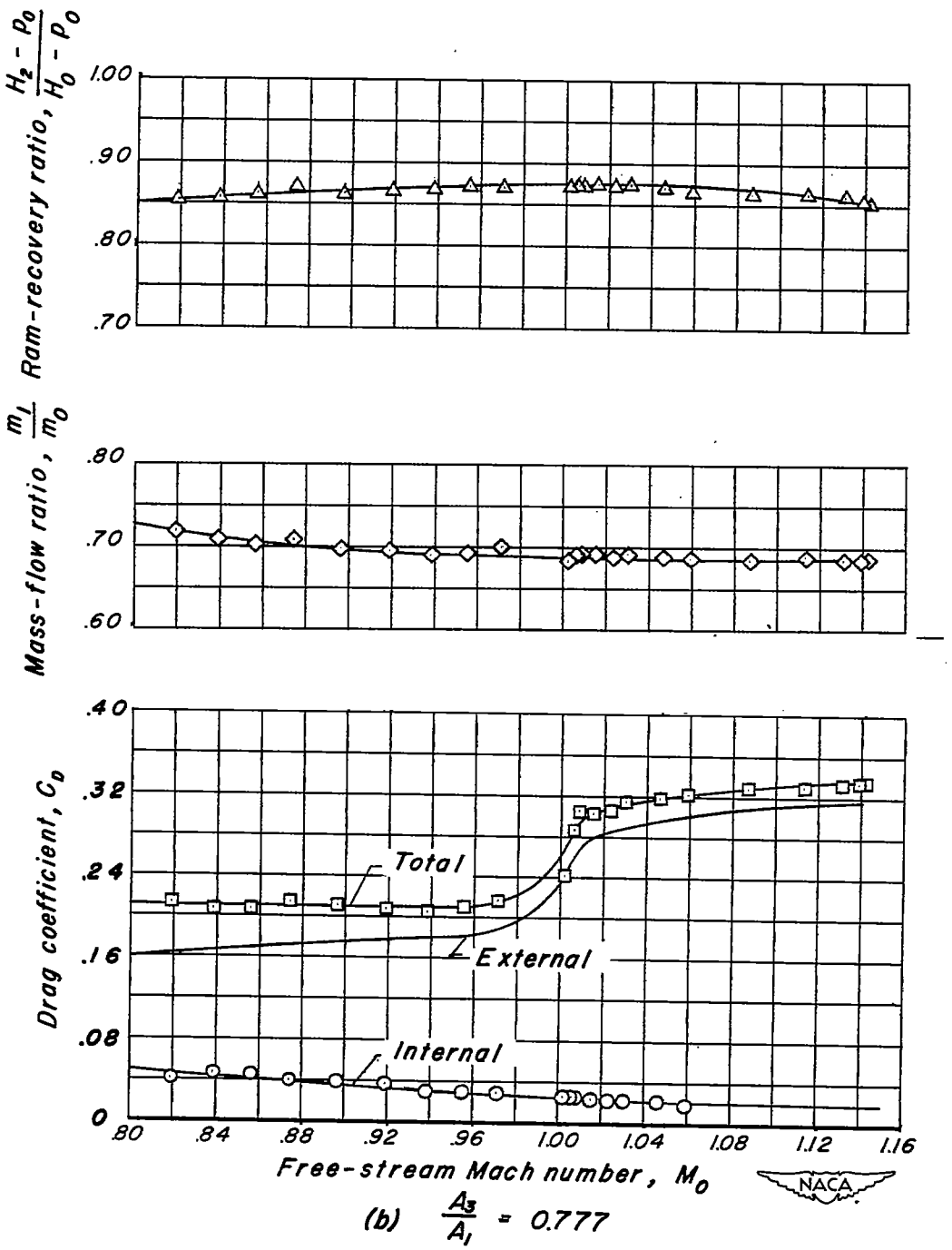

(b) $\frac{A_3}{A_1} = 0.777$

Figure 13. — Continued.

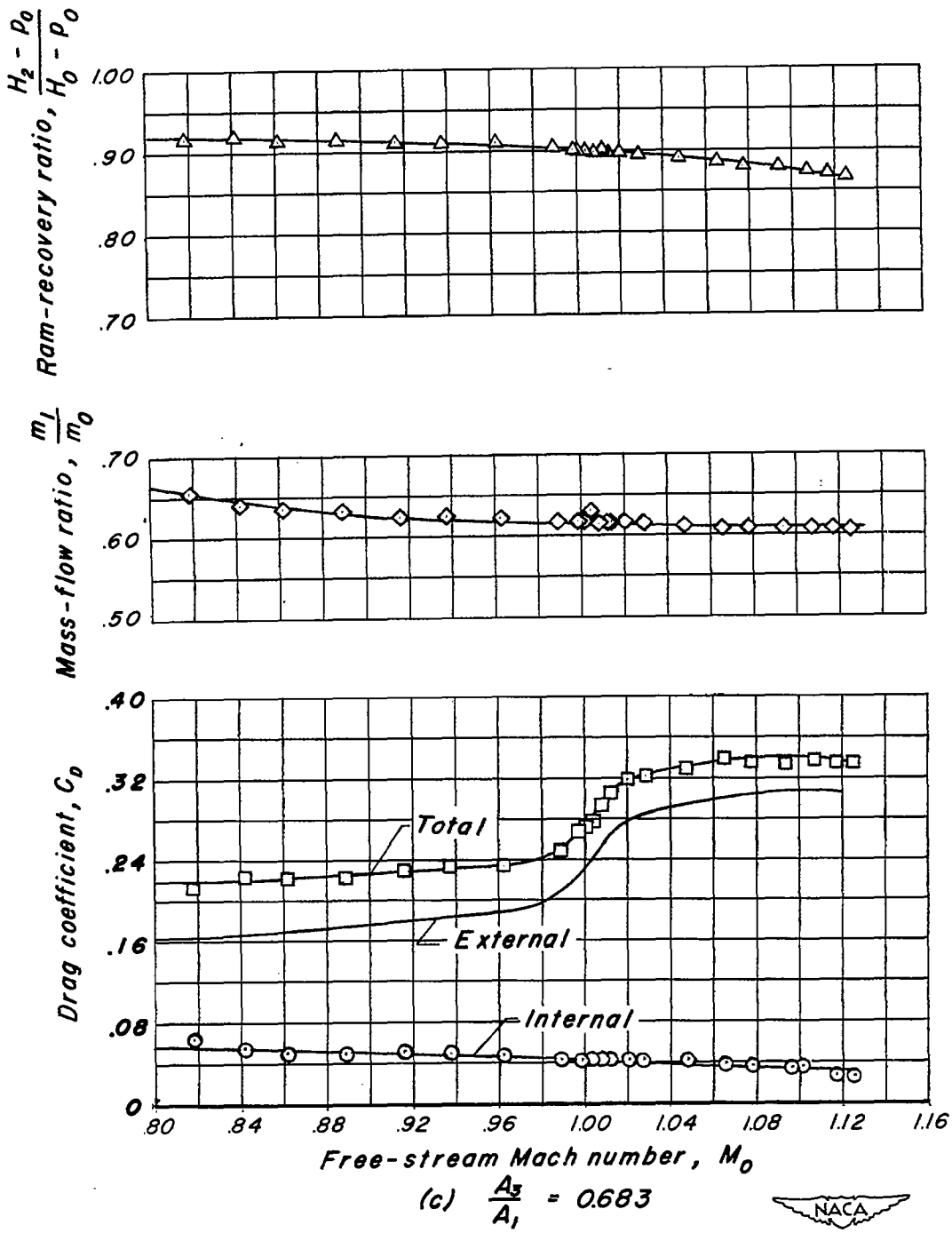

Figure 13. — Continued.

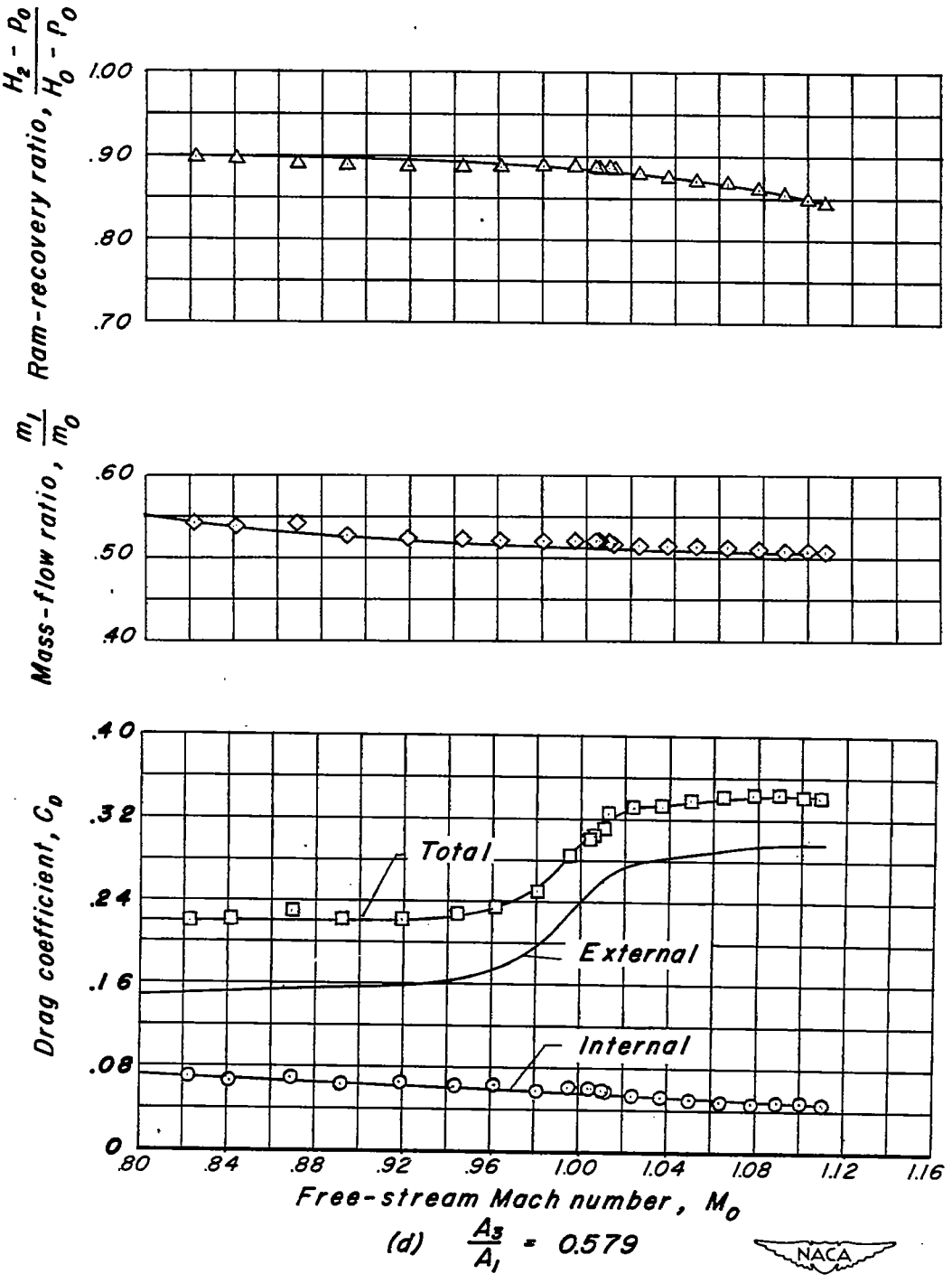

Figure 13. — Continued.

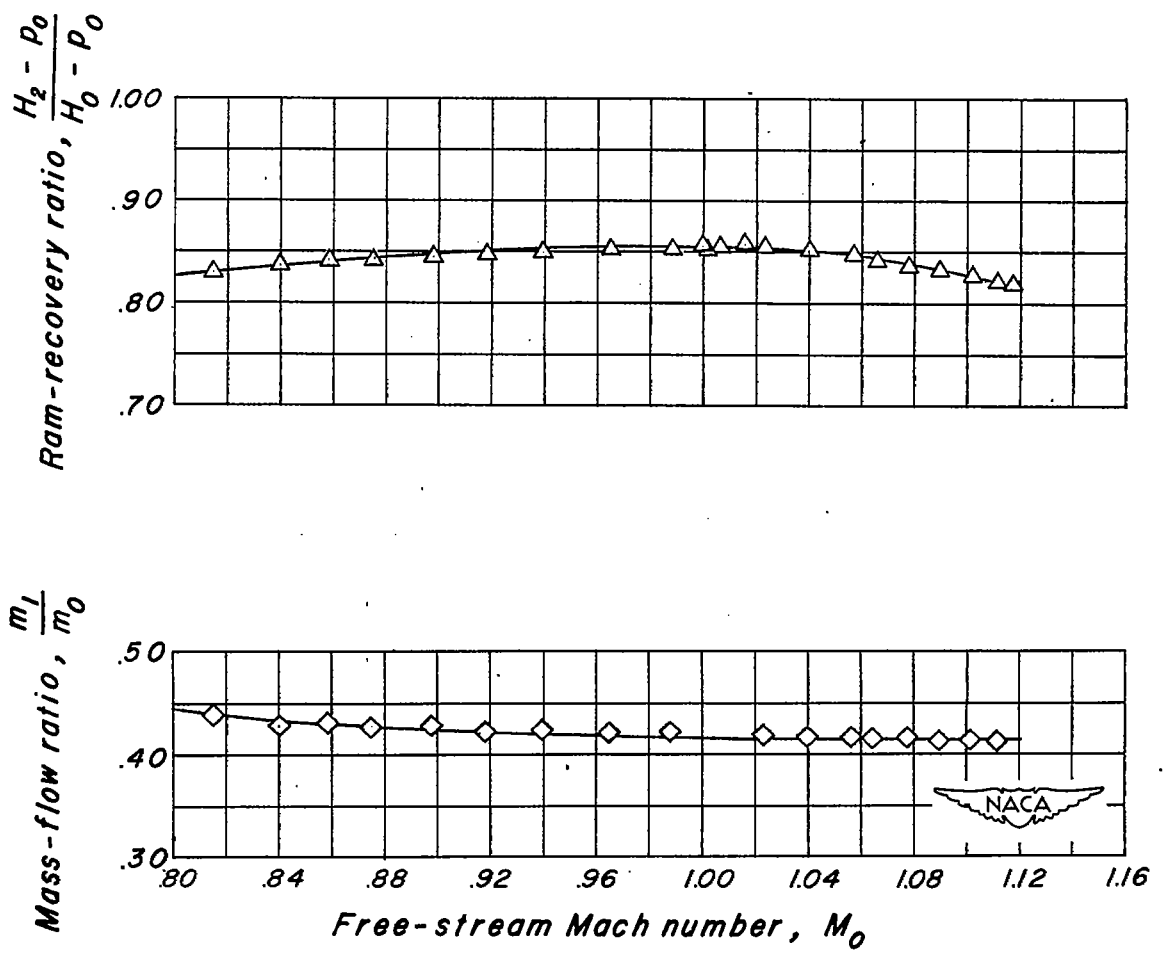

(e) $\frac{A_3}{A_1} = 0.477$

Figure 13. — Concluded.

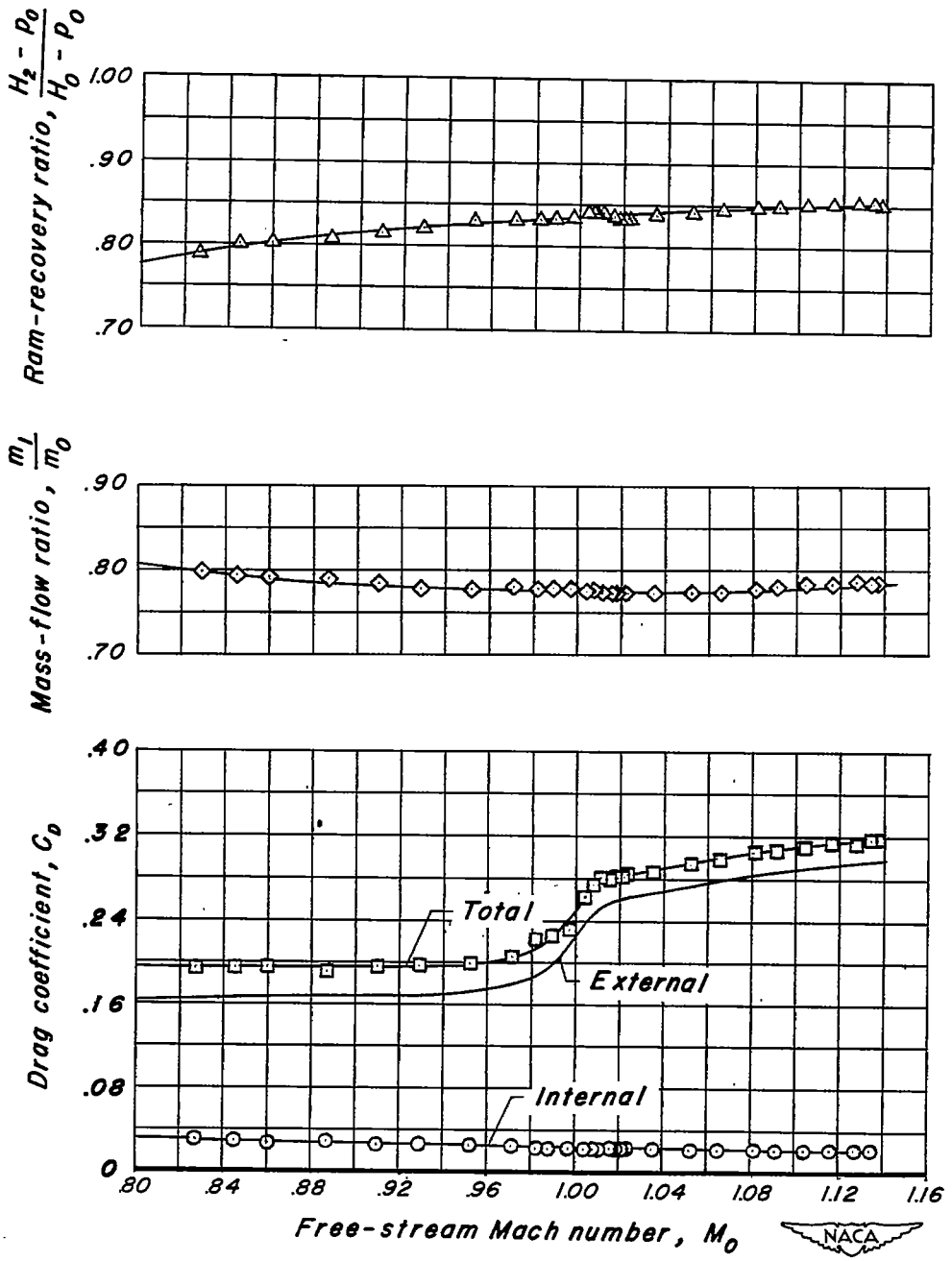

(a) $\frac{A_3}{A_1} = 0.889$

Figure 14.— Variation of drag coefficients, pressure recovery, and mass-flow ratio with free-stream Mach number for nose-inlet model.

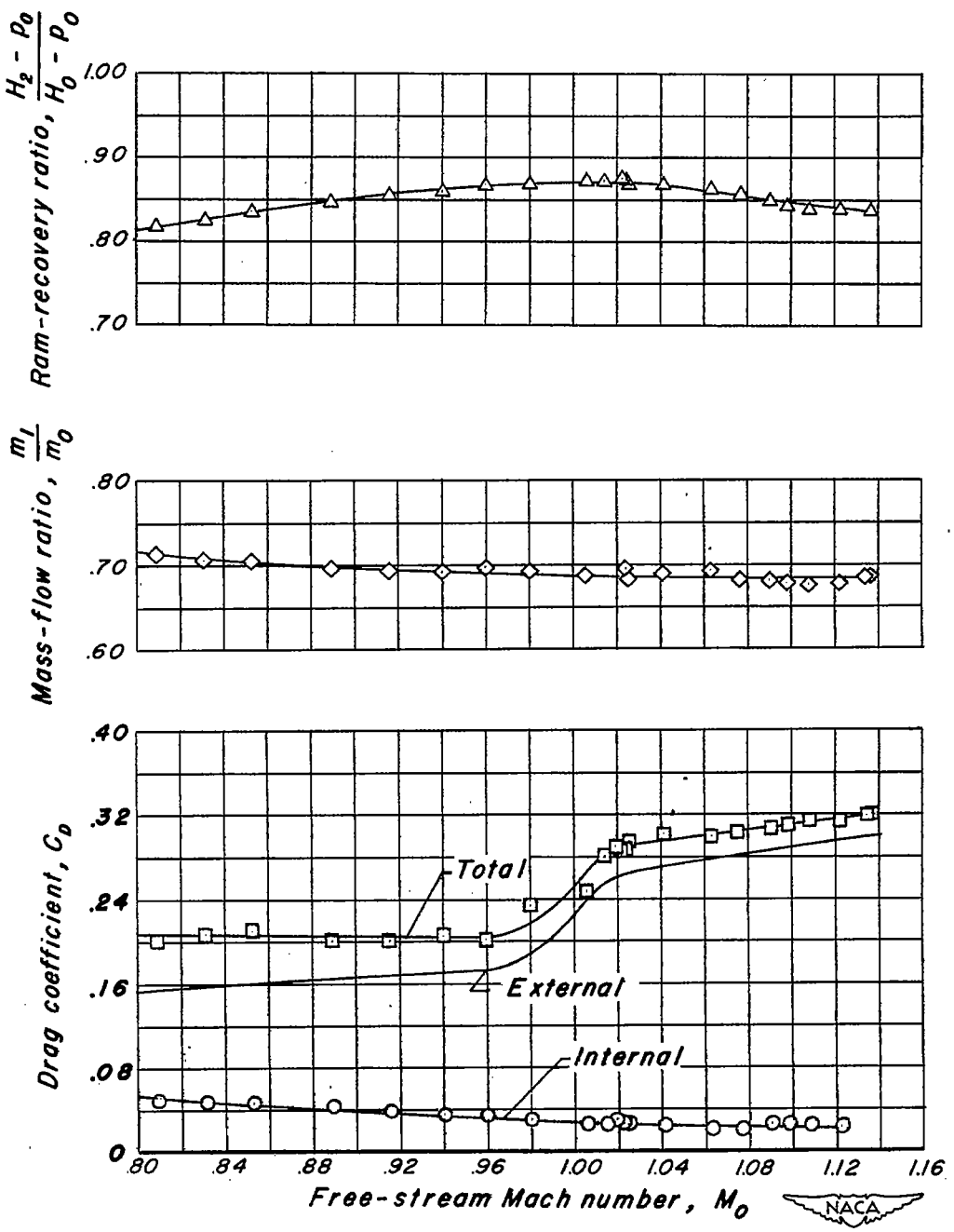

(b) $\frac{A_s}{A_1} = 0.777$

Figure 14.– Continued.

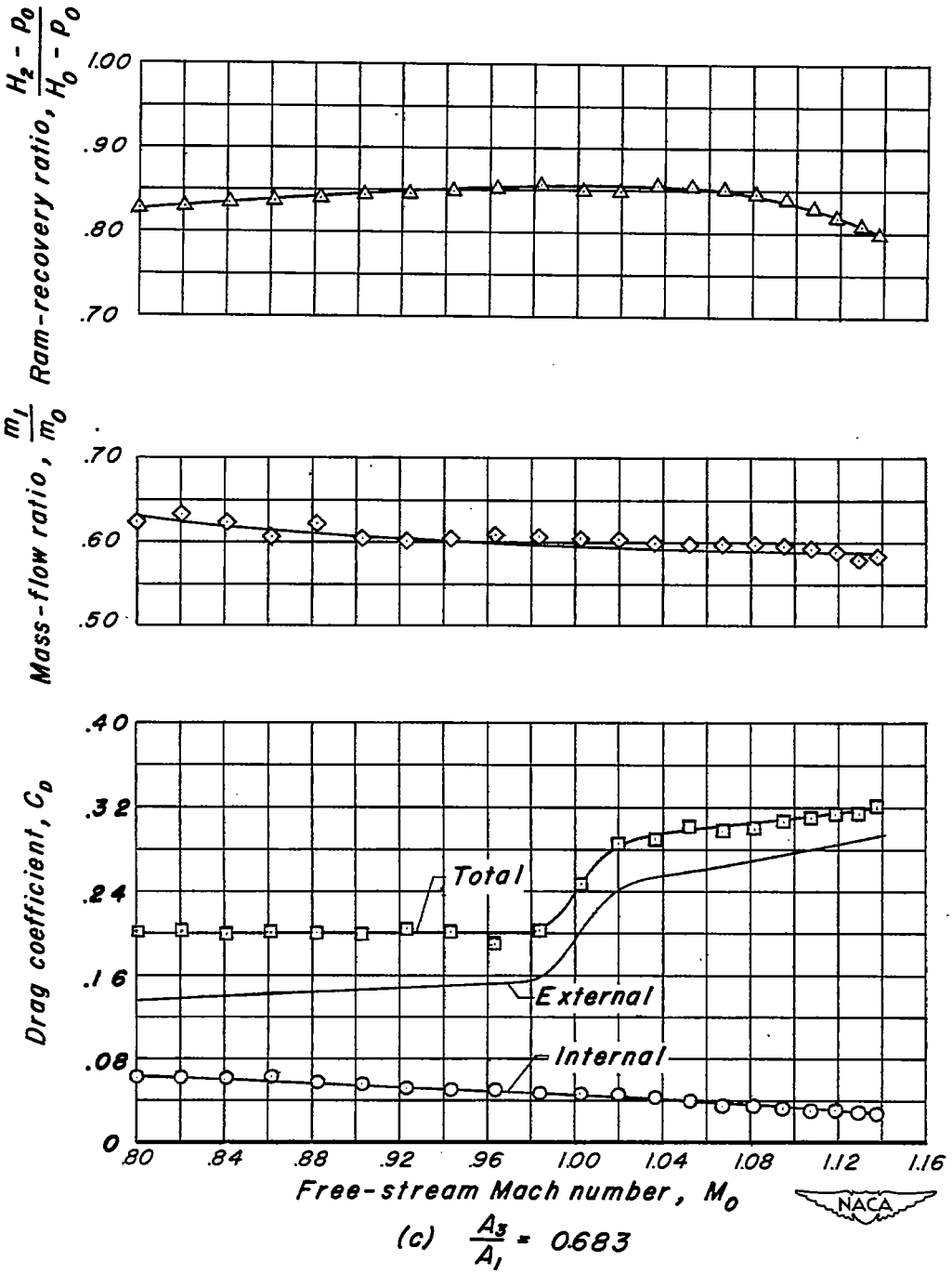

(c) $\frac{A_3}{A_1} = 0.683$

Figure 14.—Continued.

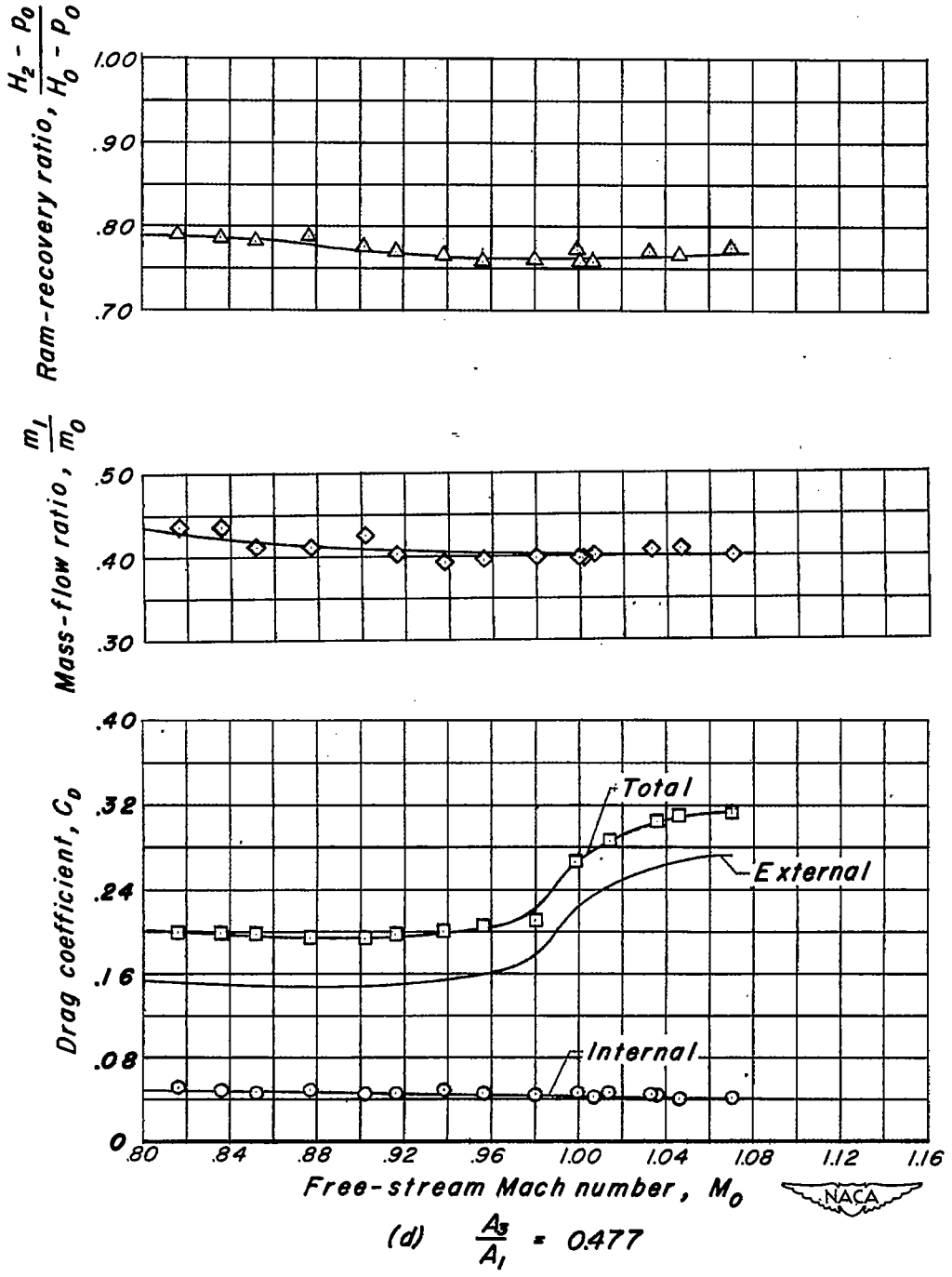

Figure 14. – Concluded.

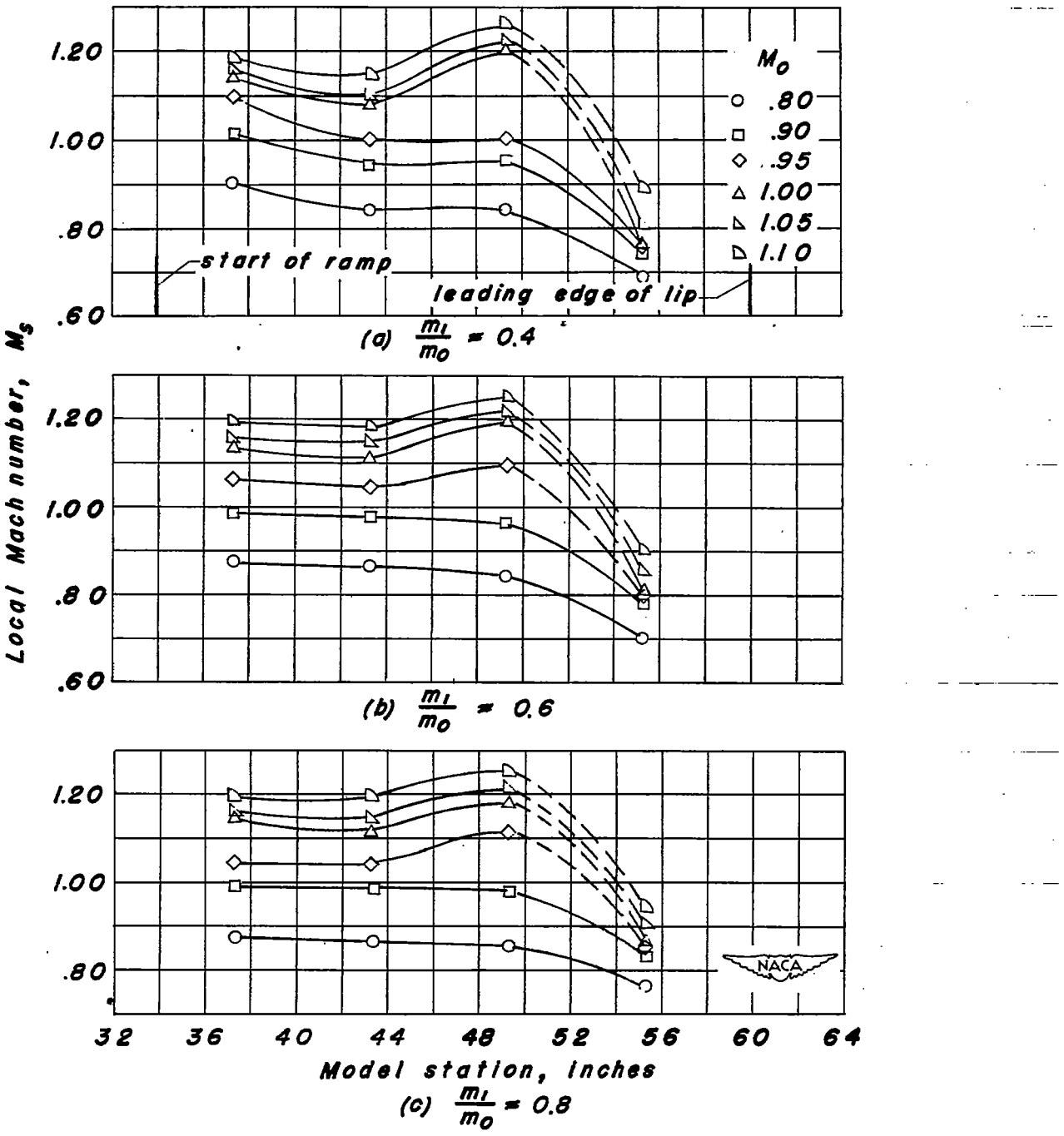

Figure 15. — Mach number distribution along ramp of submerged inlet at mass-flow ratios of about 0.4, 0.6, and 0.8.

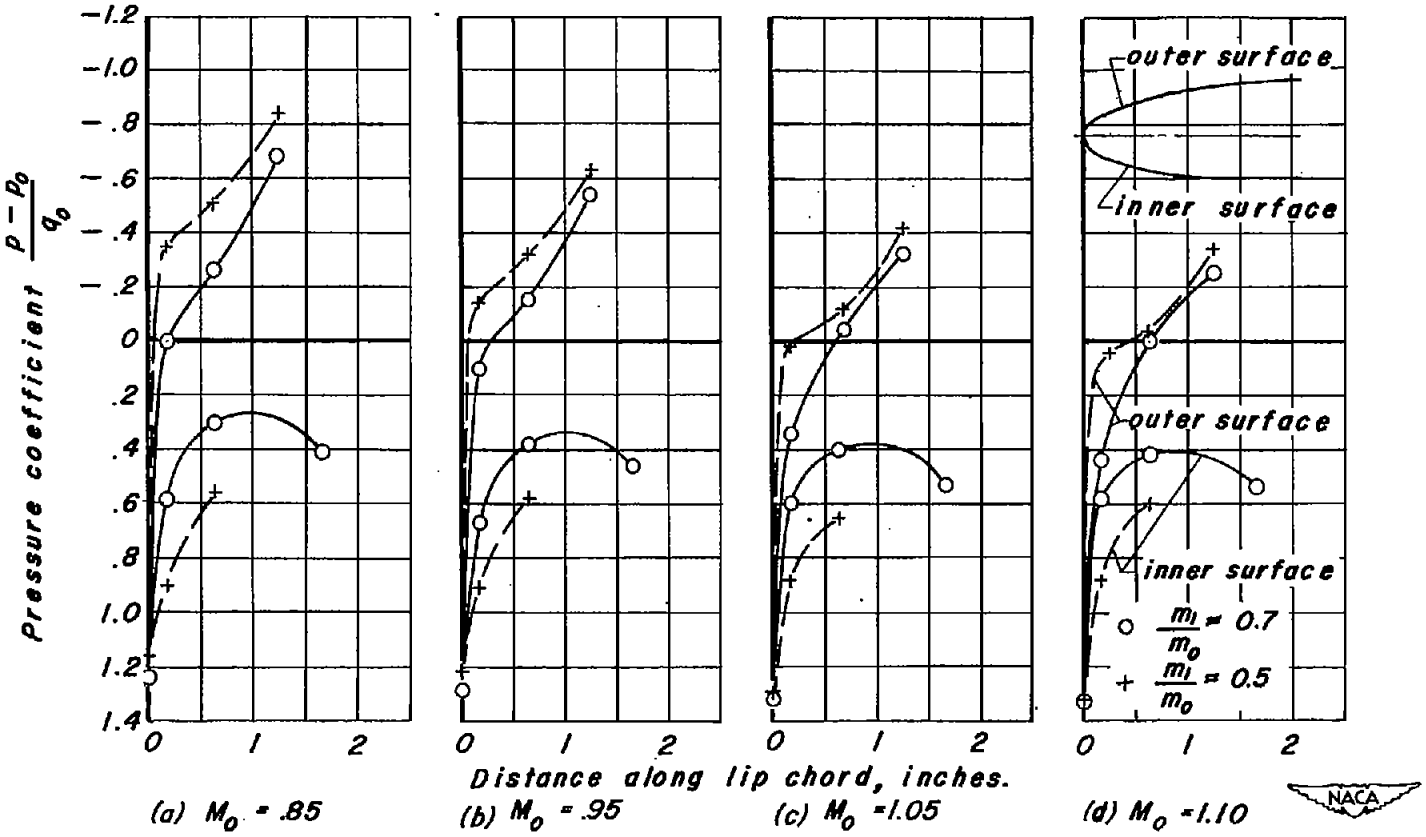

Figure 16.— Pressure distribution on lip of submerged-inlet model at mass-flow ratios of about 0.5 and 0.7.

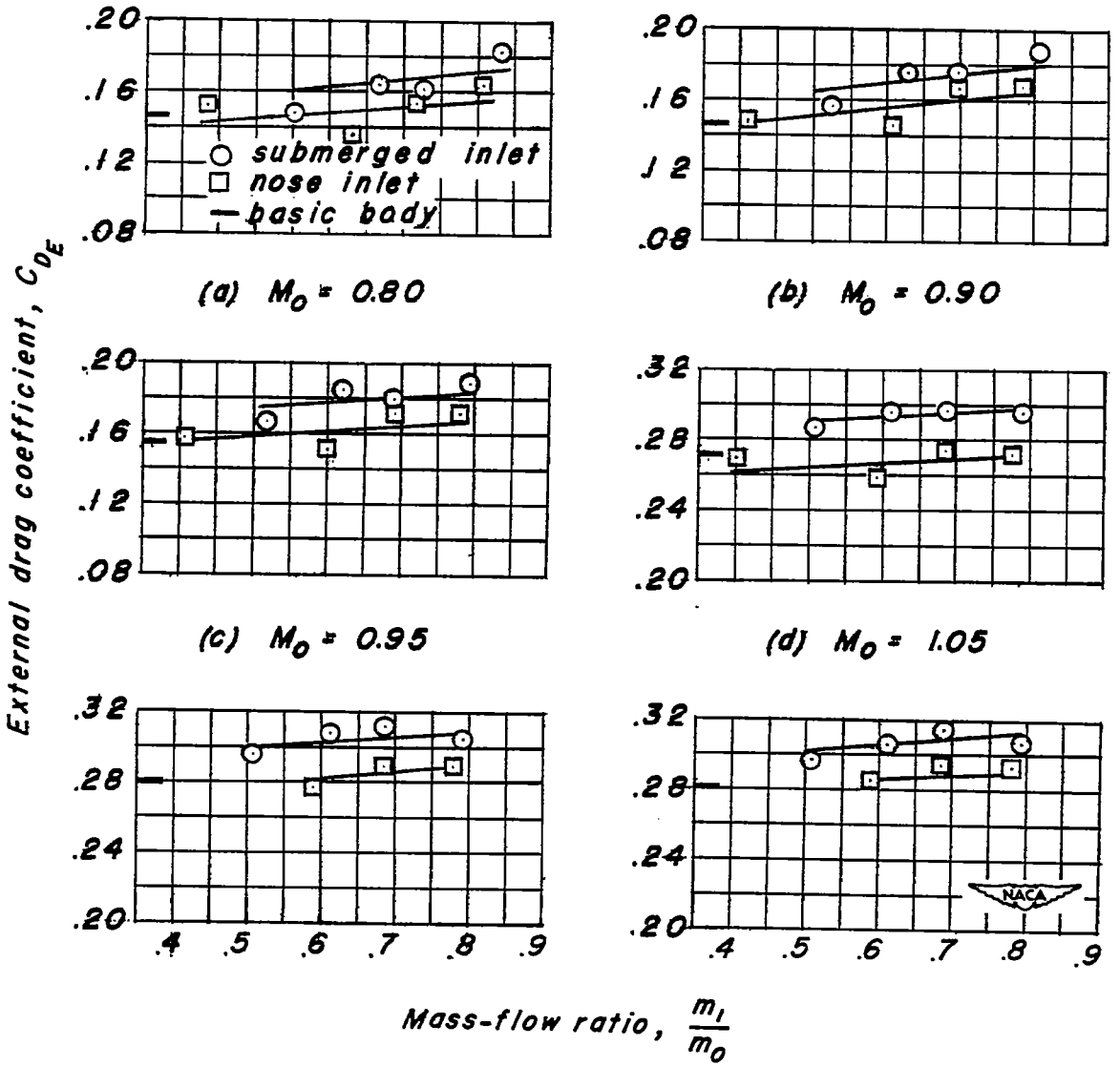

Figure 17. — Variation of external drag coefficient of inlet models with mass-flow ratio at various Mach numbers.

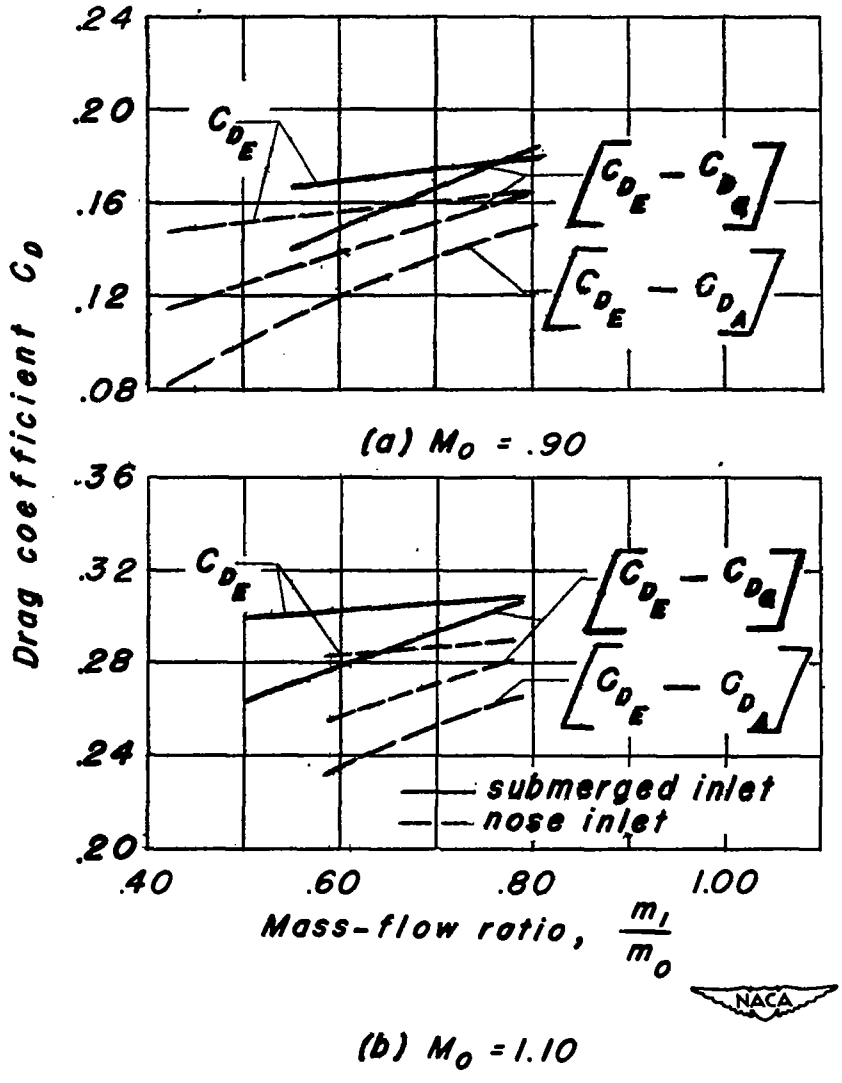

Figure 18. – Variation with mass-flow ratio of external-drag less inlet incremental-drag coefficient for inlet models and external-drag less additive-drag coefficient for nose-inlet model.

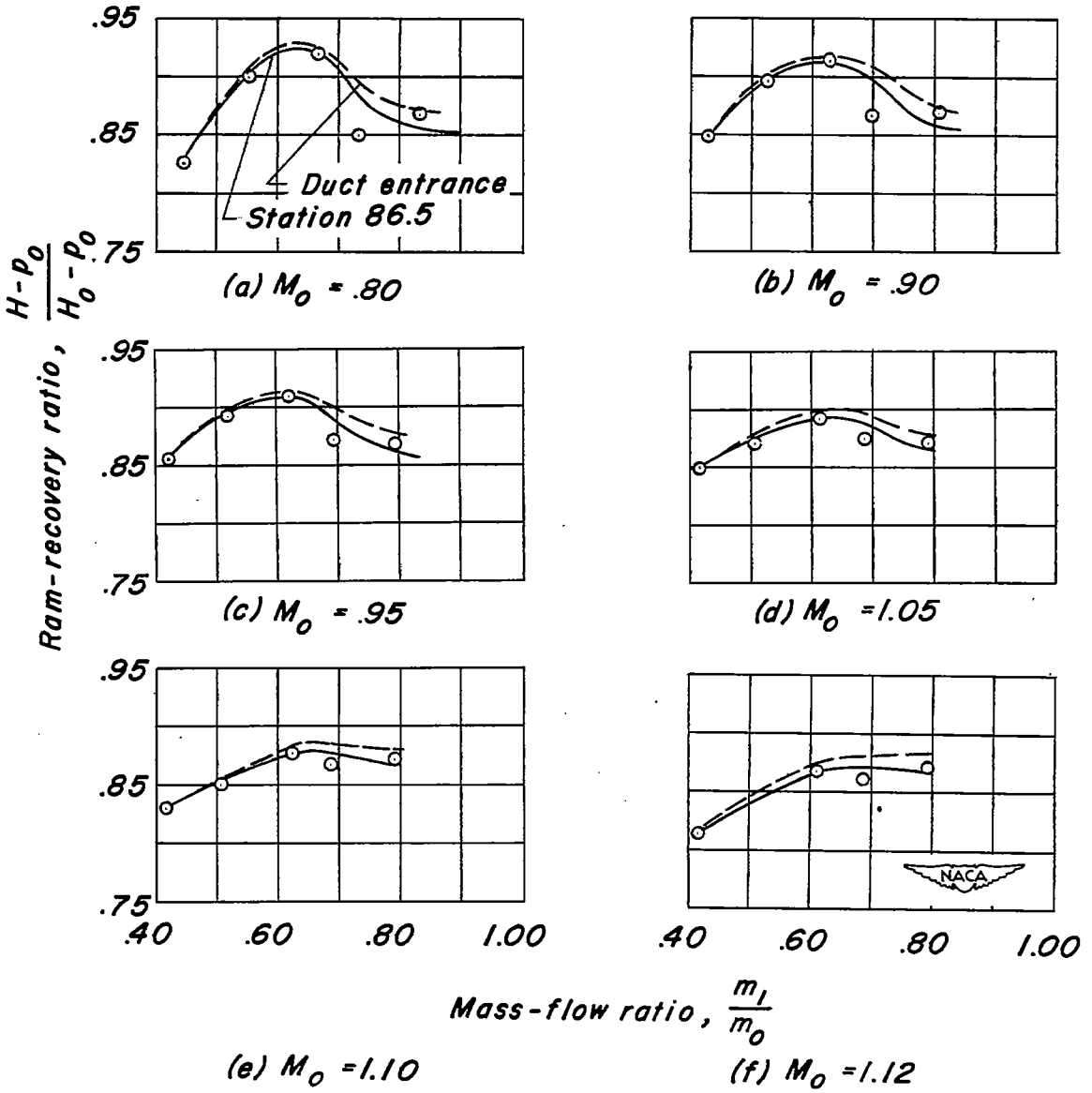

Figure 19. — Variation of ram-recovery ratio of submerged inlet with mass-flow ratio at various Mach numbers.

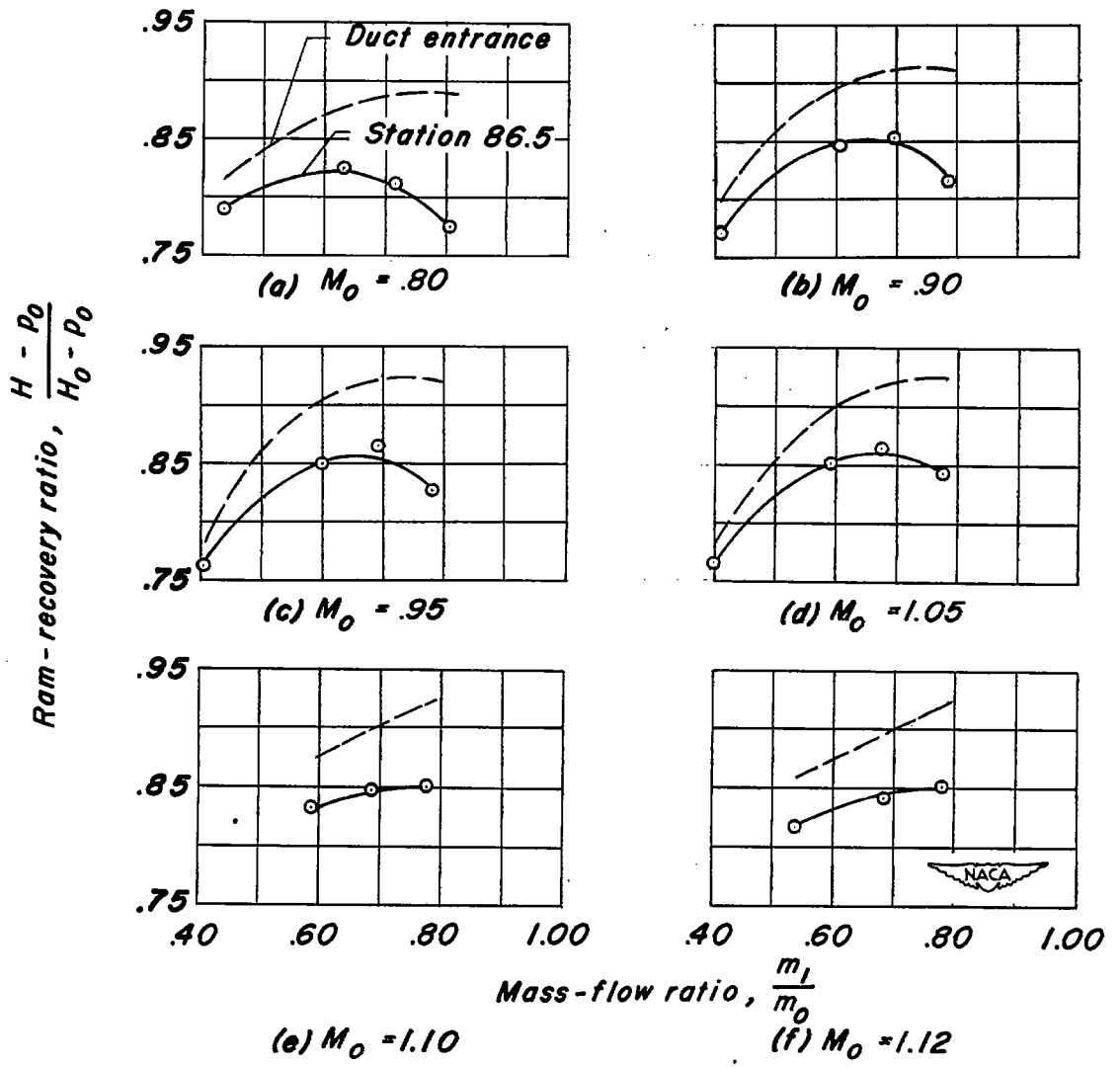

Figure 20.– Variation of ram-recovery ratio of nose-inlet model with mass-flow-ratio at various Mach numbers.

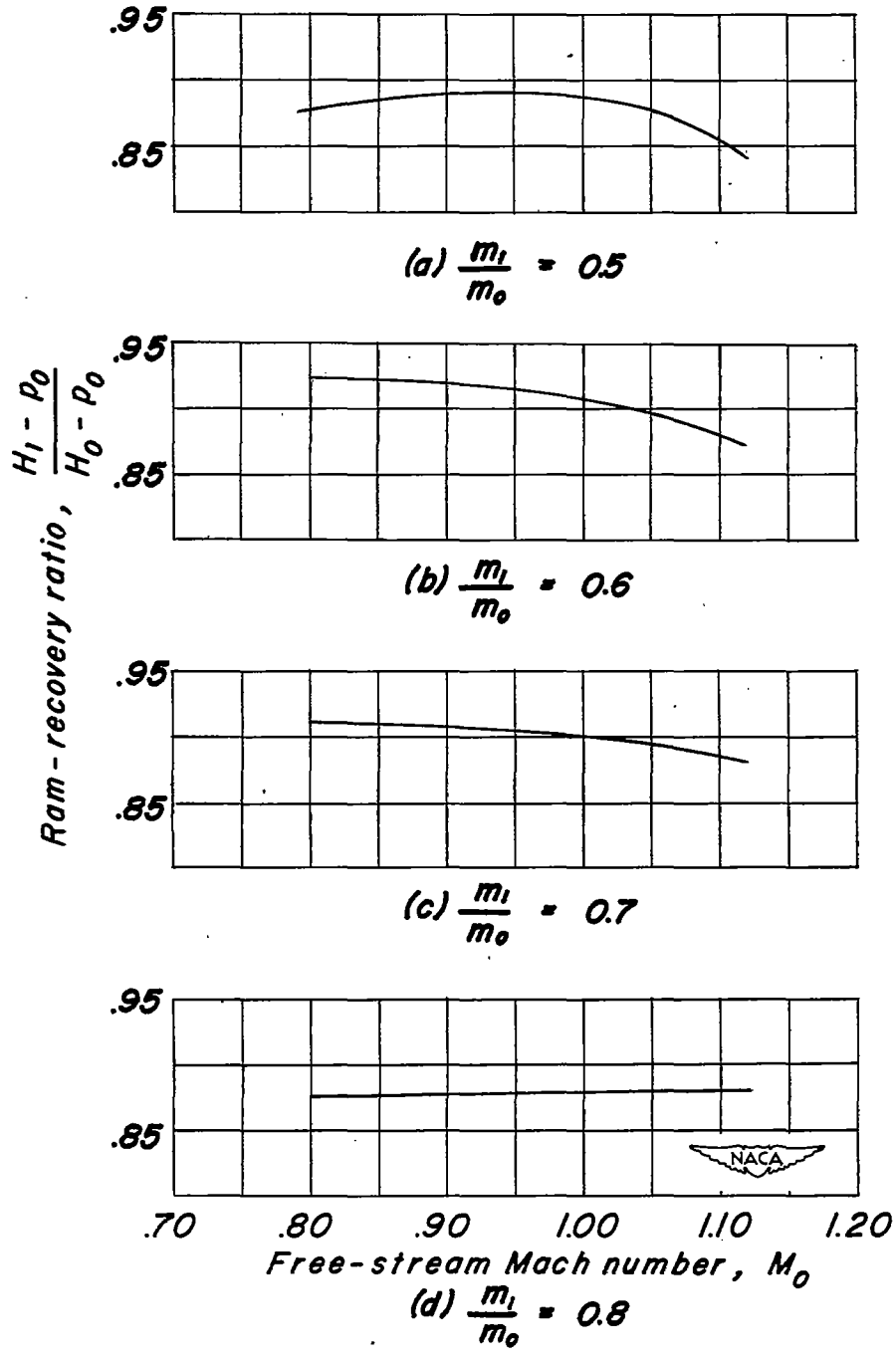

Figure 21. — Variation of entrance ram-recovery ratio with Mach number at various mass-flow ratios for the submerged inlet.

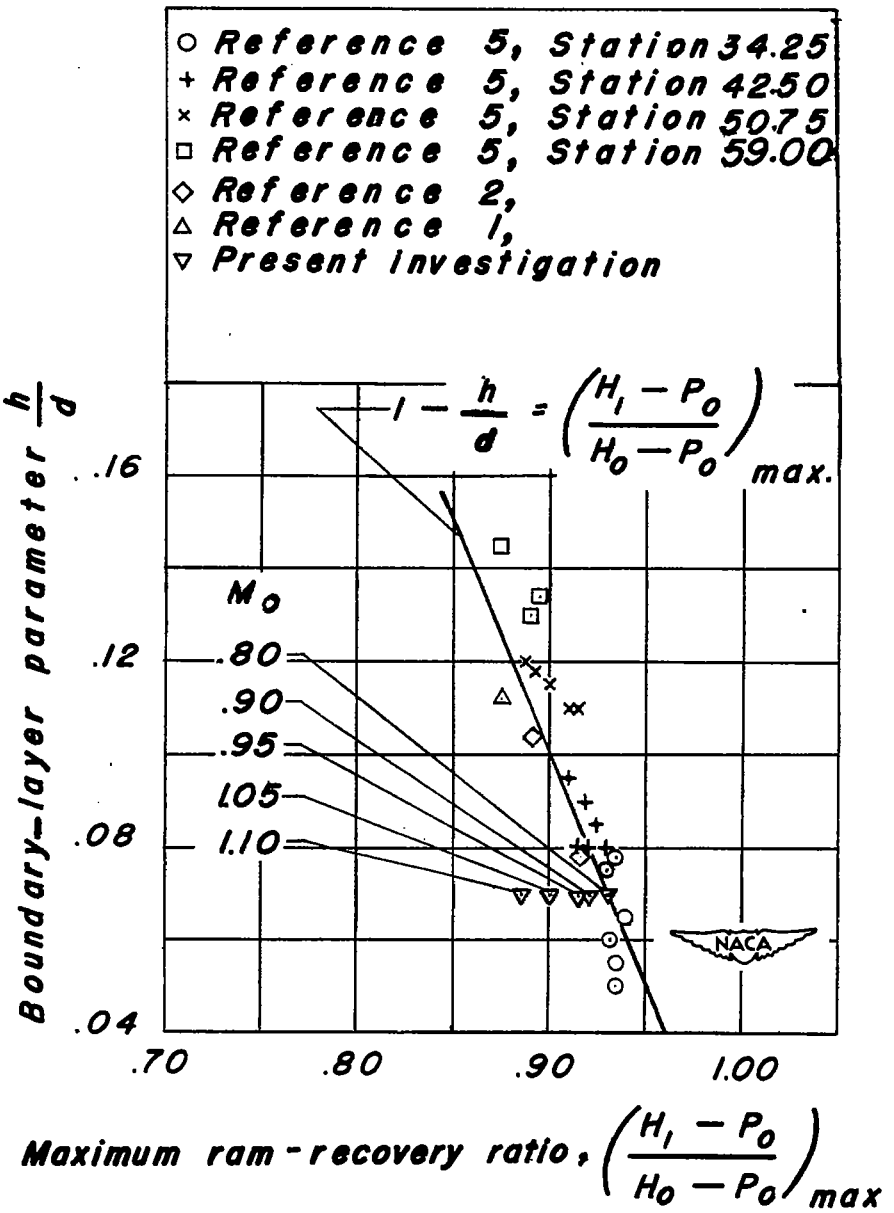

Figure 22.—Comparison of maximum ram-recovery ratio of submerged inlet with previous subsonic results.

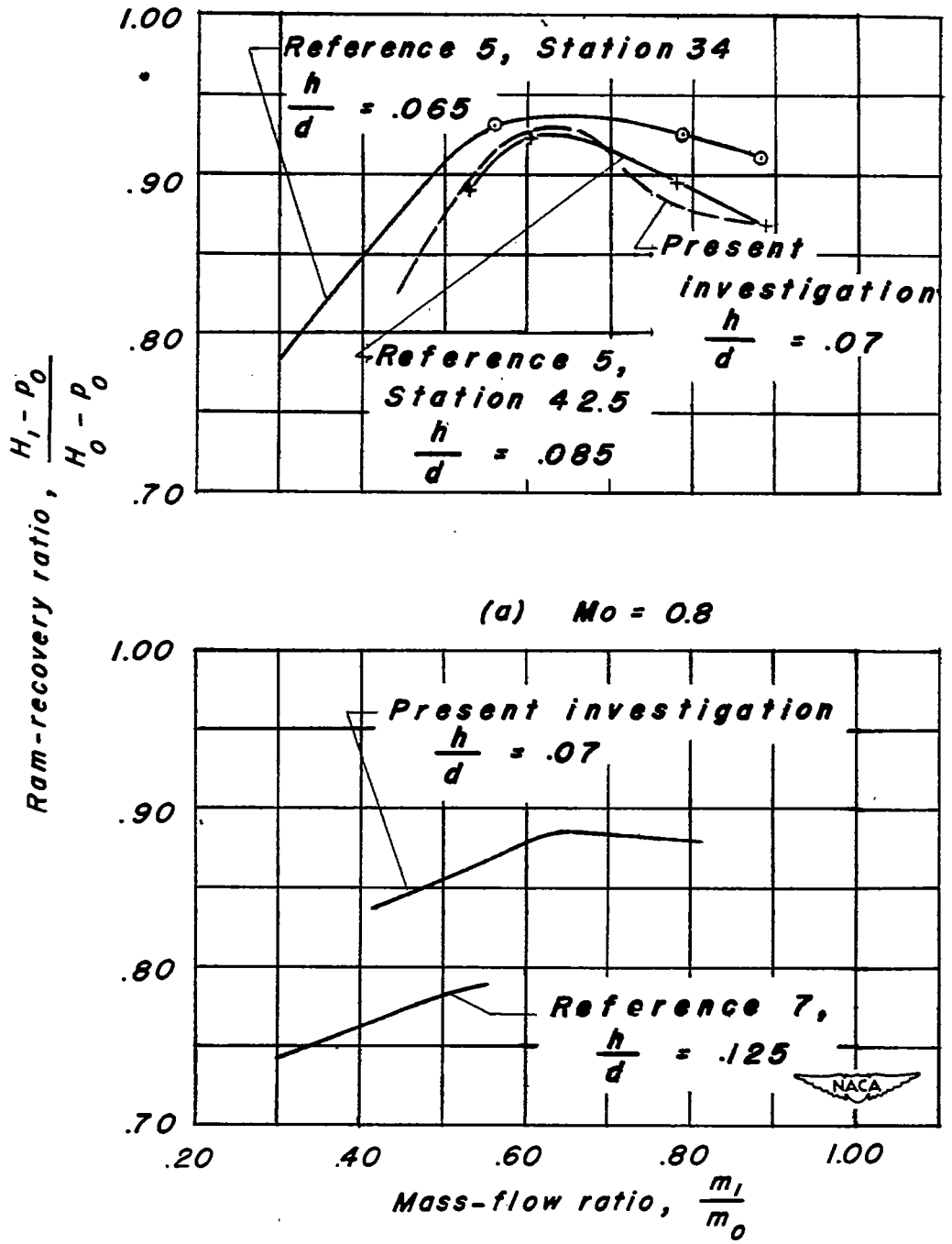

Figure 23. — Comparison of variation of ram-recovery ratio with mass-flow ratio of submerged-inlet model with previous data.

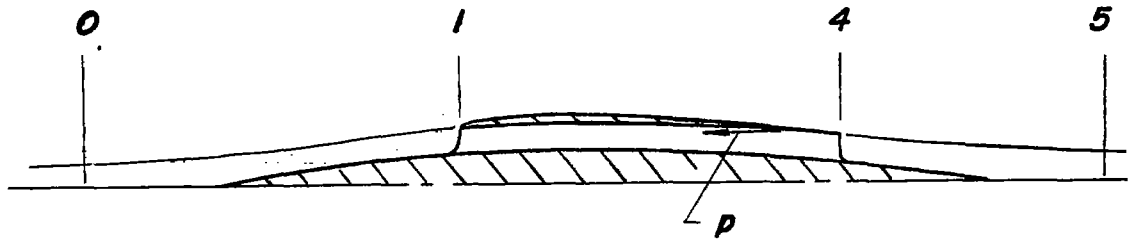

(a) Flow through a ducted body

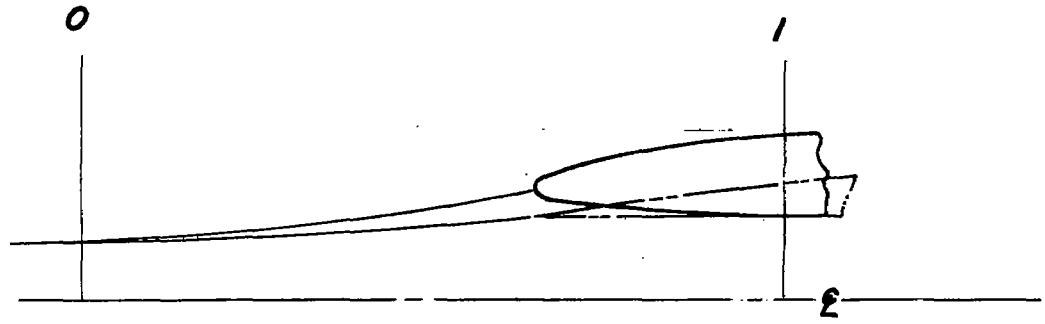

(b) Flow ahead of inlet for round lip and sharp lip

Figure 24.— Two-dimensional flow through a ducted body and ahead of an inlet.

NACA-Langley - 12-28-51 - 450